Sustainable Marine Structures

https://journals.nasspublishing.com/index.php/sms

ARTICLE

Mooring Fatigue Lifetime of Point-Absorber Wave Energy Converters in Monsoon Climates: Gulf of Thailand and Andaman Sea

Kornpaphop Ruttanawijit [1] , Yodchai Tiaple [2] , Noppong Sritrakul [3*]

[1] Department of Energy Technology, Faculty of Engineering and Industry Technology, Rambhai Barni Rajabhat University, Chanthaburi 22000, Thailand

[2] Department of Maritime Engineering, Faculty of International Maritime Studies, Kasetsart University, Sriracha Campus, Chonburi 20230, Thailand

[3] Department of Mechanical Engineering, Faculty of Engineering and Industrial Technology, Silpakorn University, Sanam Chandra Palace Campus, Nakhon Pathom 73000, Thailand

ABSTRACT

Mooring failure is a leading structural barrier to wave energy converter (WEC) commercialisation, and fatigue—rather than ultimate strength—governs mooring service life. Yet all published WEC mooring fatigue studies use North Sea or North Atlantic wave climates; no region-specific estimate exists for the monsoon-dominated waters of Southeast Asia. This study presents the first mooring fatigue lifetime assessment for the RM3 reference point absorber under the contrasting wave climates of the Gulf of Thailand and the Andaman Sea. A Dirlik frequency-domain framework—validated for bimodal RM3 mooring loads against time-domain rainflow counting by Martinez-Puente et al.—is applied with site-specific H_s–T_p occurrence weighting derived from 24 years (2000–2023) of ERA5 hourly reanalysis, cross-validated against regional WAM/SWAN hindcasts. Damage is accumulated using Palmgren–Miner's rule across five sensitivity cases: base, slack, taut, biofouling, and a combined worst case. Base-case design fatigue lifetimes (DFF = 3) are 30 years at the Gulf of Thailand and 19 years at the Andaman Sea—the latter falling

*CORRESPONDING AUTHOR:

Noppong Sritrakul, Department of Mechanical Engineering, Faculty of Engineering and Industrial Technology, Silpakorn University, Sanam Chandra Palace Campus, Nakhon Pathom 73000, Thailand; Email: sritrakul_n@su.ac.th

ARTICLE INFO

Received: 27 May 2026 | Revised: 8 June 2026| Accepted: 26 June 2026 | Published Online: 21 July 2026

DOI: https://doi.org/10.36956/sms.v8i3.3356

CITATION

Ruttanawijit, K., Tiaple, Y., Sritrakul, N., 2026. Mooring Fatigue Lifetime of Point-Absorber Wave Energy Converters in Monsoon Climates: Gulf of Thailand and Andaman Sea. Sustainable Marine Structures. 8(3): 33–58. DOI: https://doi.org/10.36956/sms.v8i3.3356

below the conventional 25-year target despite its roughly threefold-greater wave resource. Seasonal damage is near-uniform between the two monsoons at the Gulf but strongly southwest monsoon-dominated (67%) at the Andaman Sea. Biofouling reduces lifetime by 23–29%, and the combined worst case drives the Andaman lifetime to 8.9 years, below the 10-year inspection threshold. The results inform inspection scheduling, mooring configuration, and design-fatigue-factor selection, demonstrating that site-specific monsoon weighting is essential for credible WEC mooring fatigue assessment in Southeast Asian waters.

Keywords: Wave Energy Converter; Mooring Fatigue; Dirlik Method; Monsoon Wave Climate; Gulf of Thailand; Andaman Sea

1. Introduction

1.1. Background and Motivation

Mooring system failure remains the leading structural barrier to wave energy converter (WEC) commercialisation [1, 2]. In contrast to ultimate-strength failure, fatigue under cyclic ocean loading is the principal mechanism governing the service life of mooring components, with failures occurring at stress levels well below the material yield strength [3, 4]. Reliable lifetime estimation methodologies are therefore essential to support both the optimisation of inspection and maintenance schedules and the avoidance of structural oversizing that would compromise WEC economic performance [3]. The current body of published WEC mooring fatigue assessments is [4–6], however, almost exclusively grounded in the wave climates of the North Sea and the North Atlantic—open-ocean, mid-latitude, broadly unimodal environments characterised by sustained moderate-to-high wave energy throughout the year. The Southeast Asian monsoon-dominated waters of the Gulf of Thailand and the Andaman Sea exhibit a fundamentally different climatology: extended calm periods punctuated by intense monsoon episodes, with strong seasonal asymmetry between the northeast (NE) and southwest (SW) monsoons. Thailand's Alternative Energy Development Plan (AEDP) explicitly identifies ocean renewable energy as a target sector, yet no region-specific structural assessment has, to the present authors' knowledge, been published. Although the broader floating-offshore-renewables sector has matured rapidly, with recent reviews documenting the current status and design trends of mooring systems for floating offshore wind turbines [7, 8] and the mooring and platform design of nearshore floating solar photovoltaic systems, which have likewise been the subject of recent reviews [9], these advances have not been transferred to point-absorber WECs operating in tropical, monsoon-dominated waters. The structural design challenge therefore is not whether the wave-energy resource is sufficient in absolute terms—both sites have been characterised in resource terms by regional hindcasts [10–14]—but whether a candidate mooring system can survive the specific load history imposed by the local wave climate for a commercially viable service life. The present study addresses this question for the first time.

1.2. Literature Review and Research Gap

The relevant literature can be organised as a funnel from global studies of WEC mooring fatigue, through the methodological choices that inform the assessment, to the regional wave-climate datasets available for Thai waters, and finally to the gap in connecting these to a structural assessment. **Table 1** summarises this literature funnel and the identified gap.

Table 1. Funnel summary of the relevant literature and the identified gap.

Level	Representative References	Identified Status
Global WEC mooring	Thies et al. [4]; Xu et al. [5]; Ma et al. [6]	Conducted in the North Sea/North Atlantic context only

Table 1. *Cont.*

Level	Representative References	Identified Status
Fatigue methodology	Martinez-Puente et al.[15]; Dirlik[16]; Benasciutti[17]	Method validated for bimodal WEC loads; applied with uniform sea-state weighting only
Regional Thai wave climate	Kanbua et al.[12]; Ekphisutsuntorn et al.[13]; Kaewsai-nguan et al.[14]; Foyhirun et al.[11]; Kompor et al.[10]	Climate well characterised; not connected to structural/fatigue analysis
Identified gap	— None —	No mooring fatigue lifetime estimates for WECs in monsoon-dominated Southeast Asian waters

Global WEC mooring fatigue studies. Thies et al.[4] established the dominance of fatigue (rather than ultimate strength) in WEC mooring failure modes through analysis of multiple deployed devices. Xu et al.[5] presented a comprehensive review of mooring system design for WECs, while Ma et al.[6] provided foundational material on mooring fatigue analysis applicable to floating offshore systems generally. All three studies use North Sea or North Atlantic wave conditions as the baseline climate. More recent studies extend the WEC mooring problem in complementary directions: Zhang et al.[18] performed CFD-based dynamic coupling analysis for catenary-moored point absorbers; Lou et al.[19] reported a field-validated multi-catenary spread mooring fatigue assessment for a wave energy test berth; Xu et al.[20] proposed a deep-learning surrogate for long-term mooring tension prediction; and Abdellatef et al.[21] characterised the wear of belt-type mooring components. None of these studies addresses monsoon-dominated Southeast Asian wave climates. Frequency-domain fatigue assessment methodology. Time-domain rainflow counting (RFC)[22, 23] is the de facto reference method for fatigue damage assessment, but its computational cost makes it impractical for the large numbers of sea states required to characterise a full operational region. Frequency-domain approaches based on spectral moments offer a faster alternative[16, 17]. Multiple spectral approaches have been compared in the literature[15, 24]; the Dirlik method[16] has emerged as the most accurate for the bimodal stress processes typical of WEC mooring loads, with Martinez-Puente et al.[15] demonstrating a mean damage error of 8% relative to RFC for synthetic WEC tension signals. The Dirlik method is adopted here for this reason.

Regional wave climate. The wave climates of the Gulf of Thailand and the Andaman Sea have been characterised through multiple regional hindcast studies: Kanbua et al.[12] applied the WAM cycle-4 wave model to the Gulf of Thailand during Typhoon Linda 1997 (August–December 1997), validated against three GISTDA wave buoys (HHN, KCH, KSI) and one marine meteorological station, with WAM reported to underestimate the observed peak H_s of 4.06 m by approximately 20%; Ekphisutsuntorn et al.[13] applied the SWAN model to the upper Gulf for 1981–2004 with cross-validation against Petchburi and Ko Sichang buoys (correlation coefficients 0.72–0.82); and Kaewsai-nguan et al.[14] used SWAN forced by ECMWF reanalysis for both the Gulf and the Andaman Sea, validated against Jason-2/3 satellite altimetry (RMSE 0.13–0.27 m). Wave-energy resource assessments by Kompor et al.[10] and Foyhirun et al.[11] confirm that the Andaman Sea, particularly off Phuket–Phang Nga, provides substantially higher mean wave power than the Gulf of Thailand. Together, these studies provide regional climatological benchmarks but are not connected to any subsequent structural or fatigue analysis. Identified gap. No published study connects (i) the bimodal monsoon wave climatology of the Gulf of Thailand and the Andaman Sea with (ii) a quantitative WEC mooring fatigue lifetime estimate. The present study fills this gap.

1.3. Research Objectives and Novel Contributions

The three research aims are as follows:

- O1. Characterise the monsoon-dominated wave climate of the Gulf of Thailand and the Andaman Sea in a form suitable for WEC mooring fatigue analysis—specifically, the joint occurrence of significant wave height H_s and peak period T_p, disaggregated by monsoon season.
- O2. Estimate the mooring fatigue lifetime of the RM3 reference point absorber under the wave cli-

mate of each site, using the Dirlik frequency-domain method with site-specific occurrence weighting.

- O3. Quantify the sensitivity of the estimated lifetime to (a) seasonal loading patterns, (b) mooring configuration (slack vs. taut), and (c) biofouling.

The associated novel contributions are:

- C1. A first regional fatigue-lifetime estimate for WEC mooring in Thai waters, addressing both the Gulf of Thailand and the Andaman Sea on a comparable methodological basis.
- C2. A quantification of site-specific monsoon damage-accumulation patterns reveals a clear contrast—near-uniform NE/SW contributions at the Gulf of Thailand and strong SW dominance at the Andaman Sea—that informs site-specific inspection scheduling.
- C3. The first structural basis for comparing the two Thai sea regions for WEC deployment suitability, complementing existing wave-resource studies that have addressed each site in isolation.

1.4. Paper Organisation

Section 2 characterises the wave climate of the two study sites from regional hindcast and reanalysis sources. Section 3 introduces the fatigue assessment methodology—the Dirlik frequency-domain framework, the RM3 reference device, and the five sensitivity cases. Section 4 presents the computed damage distributions, lifetime estimates, and sensitivity results. Section 5 discusses the monsoon damage-concentration effect, compares the two sites for structural deployment suitability, and identifies limitations and future work. Section 6 summarises the principal conclusions.

2. Wave Climate Characterization

2.1. Study Sites

Two areas are chosen to represent the two seas of Thailand, with each area corresponding to its respective monsoon, as shown in **Figure 1**:

- Site 1—Gulf of Thailand (GoT). A central Gulf location at approximately 10.0° N, 100.0° E, with water depth of order 40–60 m. The site is sheltered from open-ocean swell by the Malay Peninsula and is dominated by wind-sea generation under the NE monsoon from November to February.
- Site 2—Andaman Sea. A western Thailand location at approximately 8.0° N, 98.0° E, water depth 50–80 m, with direct exposure to SW monsoon swell from May to September across the open Andaman basin.

These coordinates correspond to representative ERA5 grid points and are intended for climate-zone screening rather than site-specific deployment design. Site-survey-quality bathymetry and ground-truth measurements would be required for any actual pilot deployment, as discussed in Subsection 5.4.

2.2. Data Sources and Validation

Four complementary wave-climate data sources are used, summarised in **Table 2**.

For the present analysis, the ERA5 hourly reanalysis[25] is used as the primary source for the H_s–T_p joint distribution because it provides continuous, hourly hindcasts at both sites over a 24-year window (2000–2023, 210,384 hourly records per site). The regional WAM and SWAN hindcasts[13, 14] are used as cross-validation benchmarks for the annual mean H_s and seasonal pattern.

A quantitative cross-validation of the ERA5-derived statistics against the regional benchmarks is summarised in **Table 3**. The agreement is within the ±15–20% band expected of a 0.5° global reanalysis at these semi-enclosed and coastal sites: the ERA5 annual mean H_s over-predicts at the Gulf of Thailand (+17%) and under-predicts at the Andaman Sea (−18%) relative to the higher-resolution regional WAM and SWAN hindcasts, while the mean T_p and SW-monsoon mean H_s fall within the published benchmark ranges. The signed direction of the discrepancy differs between sites because the dominant error mechanisms differ—unresolved coastline sheltering inflates the open-water Gulf signal, whereas the coarse grid smooths the Andaman swell peak—so no single multiplicative bias correction is applicable. The satellite-altimeter validation RMSE of 0.13–0.27 m reported for Jason-2/3 in the regional studies provides an independent measure of the absolute accuracy achievable in these waters. These differences are carried forward as a known limitation of the absolute lifetime estimates (Subsection 5.4); the relative site comparison, which is the principal contribution of this study, is robust to a site-uniform scaling of H_s.

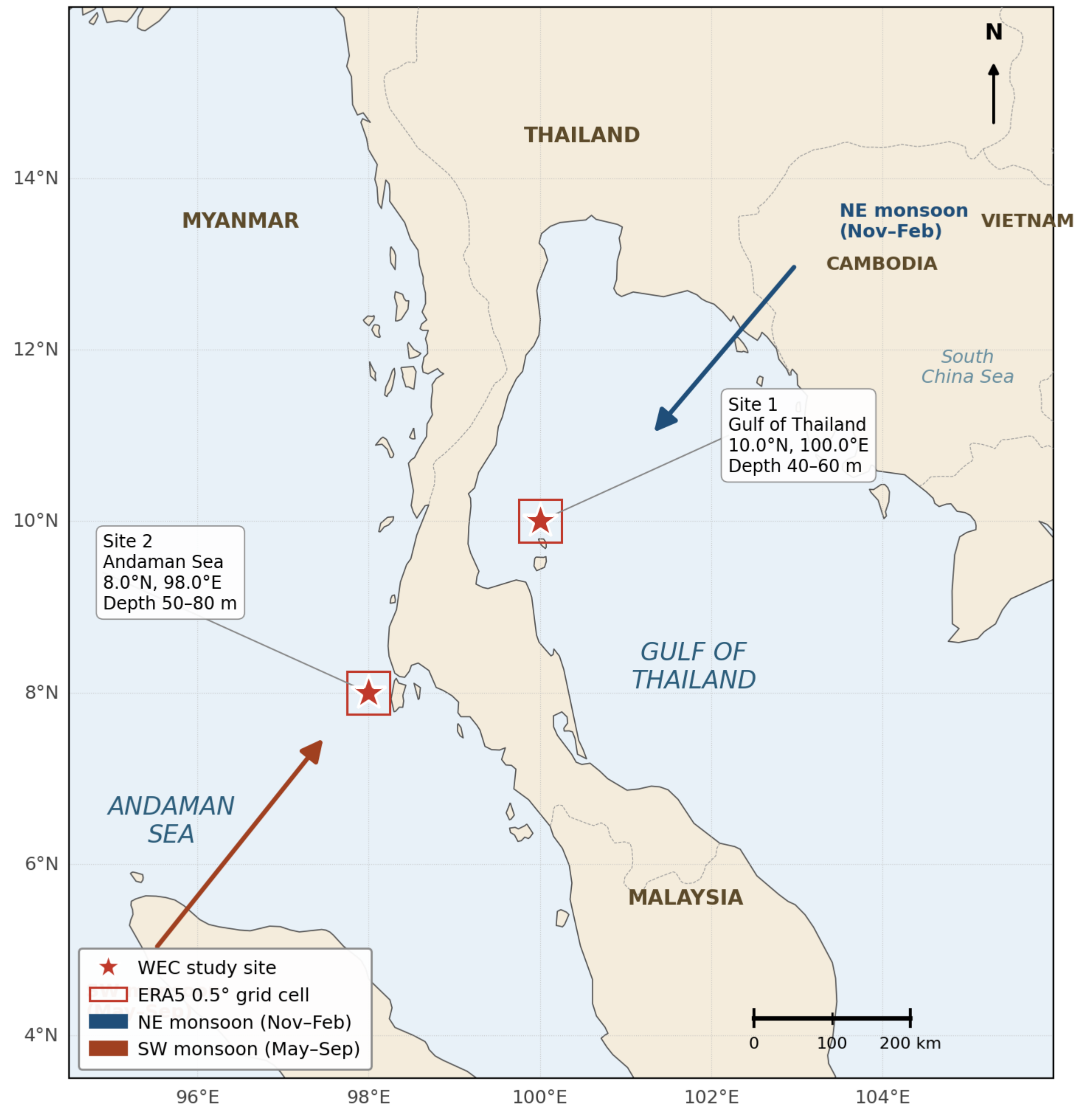

Figure 1. Study site map showing the two ERA5 grid points used in this study, regional bathymetry, and prevailing monsoon wind directions.

Table 2. Wave-climate data sources used in the present study.

Source	Coverage	Period	Validation
Kanbua et al.[12] WAM cycle-4	Gulf of Thailand	Aug–Dec 1997 (Typhoon Linda)	GISTDA buoys + NOGAPS winds
Ekphisutsuntorn et al.[13] SWAN	Upper GoT (Bangkhuntien)	1981–2004	Petchburi + Ko Sichang buoys (CC = 0.72–0.82)
Kaewsai-nguan et al.[14] SWAN	GoT + Andaman Sea (48 grid pts)	2009, 2019	Jason-2/3 altimetry (RMSE = 0.13–0.27 m)
ERA5 reanalysis (ECMWF)[25]	Both sites (0.5° wave grid)	2000–2023 hourly	Used directly for H_s/T_p extraction in the present study

Table 3. Cross-validation of ERA5-derived wave statistics against regional hindcasts and satellite benchmarks at the two study sites.

Site	Metric	Era5 (This Study)	Regional Benchmark	Diff.	Benchmark Source
Gulf of Thailand	Annual mean H_s (m)	0.56	0.48	+17%	Kompor et al. [10] (WAM)
Gulf of Thailand	Annual mean T_p (s)	4.2	3.8–4.5	within	Ekphisutsuntorn et al. [13] (SWAN)
Gulf of Thailand	Calm fraction $H_s < 0.5$ m	52%	≈73%	−21 pp	Kompor et al. [10]
Andaman Sea	Annual mean H_s (m)	0.80	0.98	−18%	Foyhirun et al. [11] (SWAN)
Andaman Sea	SW-monsoon mean H_s (m)	1.07	1.0–1.2	within	Foyhirun et al. [11]
Both sites	H_s satellite RMSE (m)	—	0.13–0.27	ref.	Jason-2/3 alt. [12, 14]

Note: Percentage differences are ERA5 relative to the benchmark; "within" denotes agreement within the published benchmark range; pp denotes percentage points.

2.3. Long-Term Wave Statistics

Seasonal wave statistics for the two sites are presented in **Table 4**, disaggregated by monsoon season (NE, SW, and transitional). The published annual mean values used as benchmarks are $H_s \approx 0.48$ m for the Gulf of Thailand with calm fraction ($H_s < 0.5$ m) of approximately 73%, and $H_s \approx 0.98$ m for the Andaman Sea with annual mean wave power approximately four times that of the Gulf.

The ERA5-derived annual mean H_s values (0.56 m for the Gulf of Thailand and 0.80 m for the Andaman Sea) agree to within 15–20% with the published regional benchmarks (0.48 and 0.98 m, respectively). A recent multi-criteria study of the Gulf of Thailand by Ruttanawijit et al. [26] using ERA5 reanalysis (2019–2023) validated against 31 in-situ stations reports comparable H_s values (0.48–0.52 m at Kaewsai-nguan et al. [14]; this is discussed further in Subsection 5.4. The Andaman Sea mean wave power computed here (2,806 W/m) is approximately 3.25× that of the Gulf of Thailand (864 W/m), broadly consistent with the ratio reported by Foyhirun et al. [11].

2.4. H_s–T_p Joint Occurrence

The joint occurrence of H_s and T_p determines the fatigue load history when each sea state is weighted by its annual probability. The full 24-year ERA5 record is binned on a $(\Delta H_s, \Delta T_p) = (0.5\,\text{m}, 1\,\text{s})$ grid covering $0 \le H_s \le 6$ m and $3 \le T_p \le 14$ s; the resulting probability matrices are used directly as the weighting $p(H_{s,i}, T_{p,j})$ in the Dirlik calculation of Section 3. The scatter for both sites is shown in **Figure 2**.

Table 4. Seasonal wave statistics at the two study sites, computed from ERA5 hourly reanalysis (2000–2023, 210,384 records per site) at the nearest grid points (10.0° N, 100.0° E for GoT; 8.0° N, 98.0° E for the Andaman Sea).

Site	Season	Mean H_s (m)	P90	P99	Max	Mean T_p (s)	Calm %	Power W/m
Gulf of Thailand	NE monsoon	0.65	1.15	1.84	2.96	4.83	42.0	1,315
	SW monsoon	0.56	0.96	1.38	2.06	3.82	48.1	729
	Transitional	0.43	0.73	1.28	2.84	3.95	71.1	500
	Annual	0.56	0.98	1.61	2.96	4.19	51.9	864
Andaman Sea	NE monsoon	0.59	0.84	1.16	1.78	9.54	38.1	1,339
	SW monsoon	1.07	1.60	2.15	3.05	9.37	3.3	4,573
	Transitional	0.61	0.96	1.71	2.63	11.22	45.8	1,785
	Annual	0.80	1.36	2.00	3.05	9.89	25.4	2,806

Note: Calm is defined as $H_s < 0.5$ m. Wave power is computed as $P = (\rho g^2/64\pi)\, H_s^2\, T_e$, with $T_e \approx 0.86\, T_p$ for $\gamma = 3.3$.

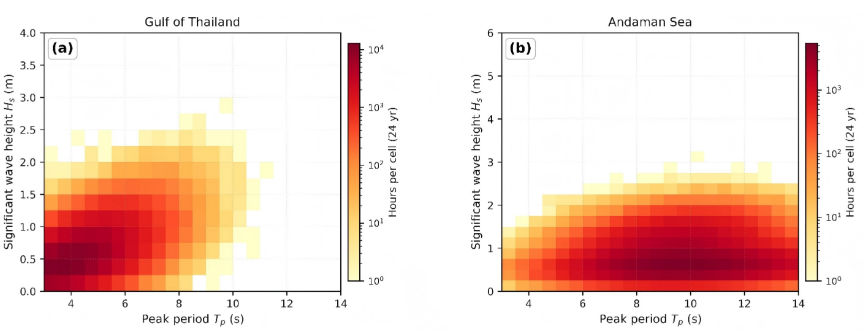

Figure 2. *Cont.*

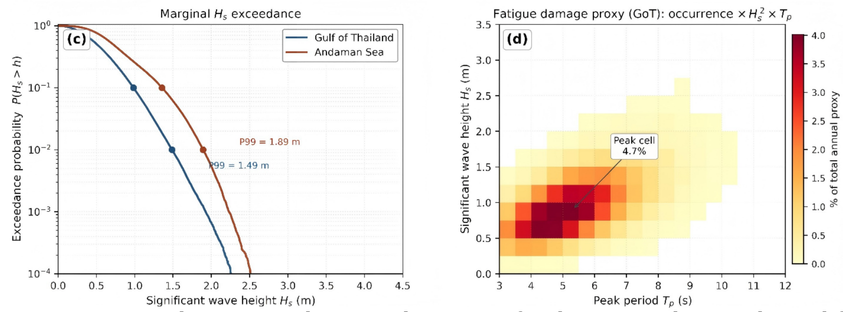

Figure 2. Joint H_s — —T_p occurrence diagrams and marginal statistics for the two study sites derived from 24 years of ERA5 hourly reanalysis.

Three observations follow:

- The GoT scatter is heavily concentrated in the $H_s < 1.0$ m, $T_p = 3–6$ s region—the wind-sea condition that dominates the annual record at this semi-enclosed basin.
- A secondary cluster representing the NE monsoon appears at $H_s = 1–2$ m, $T_p = 5–7$ s, occupying only a few percent of the annual record but corresponding to the bulk of the wave energy.
- The Andaman Sea scatter is broader and shifted toward longer peak periods ($T_p = 7–11$ s), consistent with the swell-influenced character of the SW monsoon.

For direct comparison, the H_s–T_p range covered by the 50 generic sea states used by Martinez-Puente et al.[15] ($H_s = 0.1–14$ m, $T_p = 4–18$ s) fully encompasses the GoT operational envelope, but with equal weighting per state, so that the monsoon concentration—the defining feature of the regional climate from a fatigue standpoint—is averaged out.

2.5. Monsoon Seasonality and Fatigue Relevance

The seasonal H_s statistics in **Table 4** quantify two important asymmetries. In the Gulf of Thailand, the NE monsoon mean H_s (0.65 m) exceeds the SW monsoon mean (0.56 m), and the NE monsoon calm fraction (42%) is markedly lower than the transitional period (71%). The NE monsoon contribution to wave power (1,315 W/m) is approximately 1.8× that of the SW monsoon (729 W/m). In the Andaman Sea, the SW monsoon dominates, with mean H_s (1.07 m) approximately 1.8× the NE monsoon mean (0.59 m), and a calm fraction of only 3.3%. The SW monsoon mean wave power (4,573 W/m) is approximately 3.4× the NE monsoon value. **Figure 3** shows the monthly H_s distribution for both sites, and **Figure 4** presents the corresponding fatigue-damage proxy (occurrence × H_s^2 × T_p) by sea-state cell, highlighting the cells that are expected to dominate annual fatigue damage. The seasonal distribution of fatigue damage at each site—clearly SW-dominated at the Andaman Sea and near-uniform between the two monsoons at the Gulf of Thailand—is the central regional finding of the present study and is quantified through the formal Dirlik calculation of Section 4.

The 24-year ERA5 record (2000–2023) is treated as a single stationary population for the purpose of building the H_s–T_p occurrence climatology that weights the fatigue calculation. This is a deliberate simplification. Interannual variability in the two basins is dominated by the El Niño–Southern Oscillation (ENSO) and the monsoon onset timing rather than by a secular trend: warm-phase (El Niño) years tend to suppress SW-monsoon wave energy in the Andaman Sea, while the reverse holds in cool-phase (La Niña) years. Over a 24-year window, these fluctuations are quasi-periodic and approximately mean-reverting, so the pooled occurrence distribution is a reasonable estimator of the long-term loading climate, but it does not resolve year-to-year extremes that may govern the fatigue of an individual deployment. The pooled treatment therefore yields a central-estimate lifetime rather than a worst-year bound, and the limited record length relative to the seasonal severity range is one motivation for the conservative design fatigue factor discussed in Subsection 3.5 and Subsection 5.1. The potential influence of longer-term climate-change trends on the regional wave climate—which the present stationary treatment does not capture—is addressed separately as a limitation in Subsection 5.4.

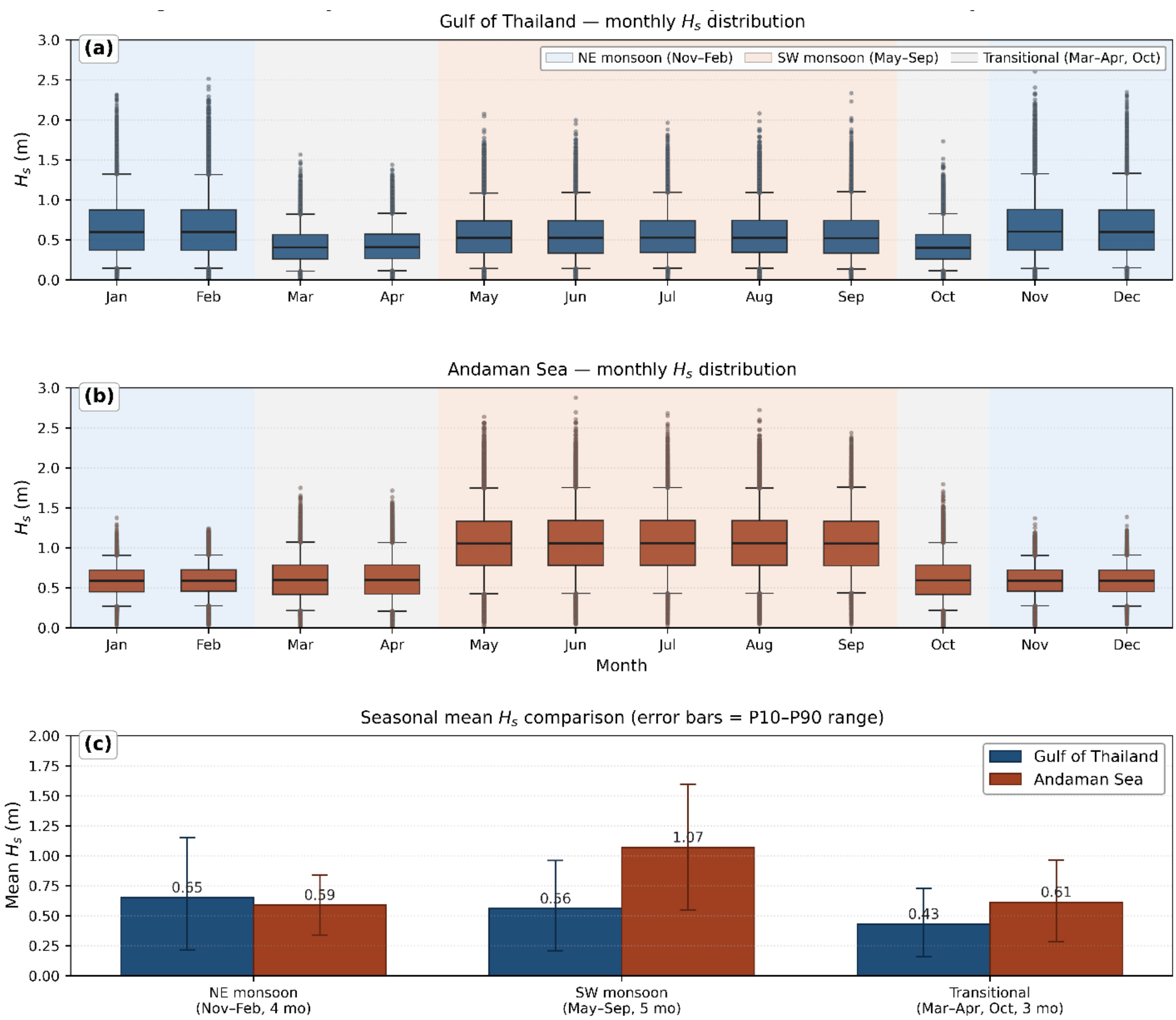

Figure 3. Monthly H_s distribution at the two sites, derived from ERA5 hourly reanalysis (2000–2023).

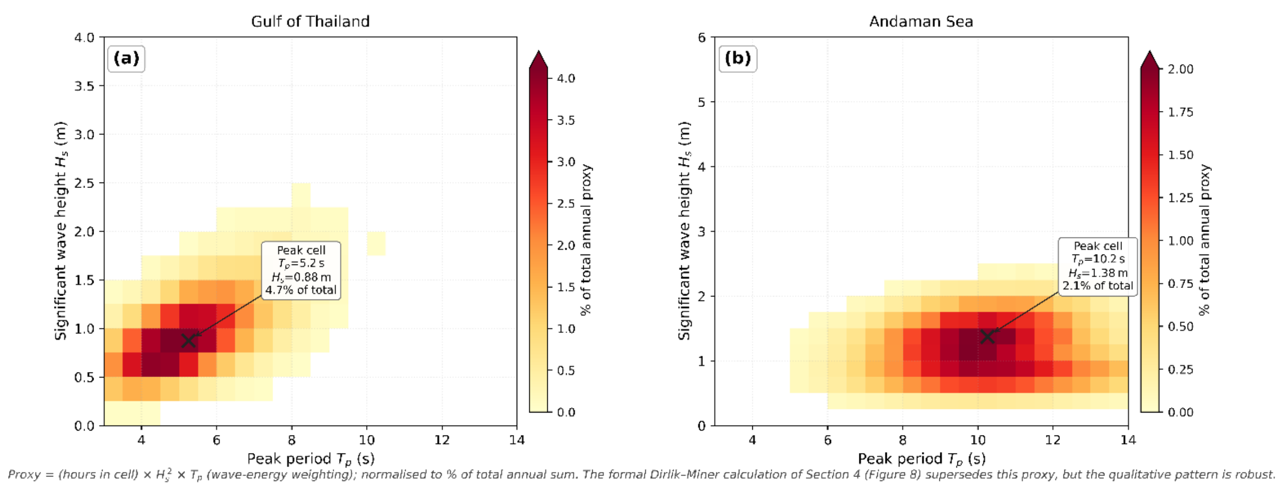

Figure 4. Fatigue damage proxy by sea-state cell. The formal Dirlik–Miner calculation of Section 4 supersedes this proxy, but the qualitative pattern is robust.

3. Fatigue Assessment Methodology

3.1. Fatigue Assessment Framework

The fatigue assessment follows the standard structural-integrity workflow: (i) characterise the material's fatigue behaviour through an S–N curve; (ii) select an appropriate fatigue indicator parameter (here, nominal stress range in the mooring chain); (iii) reconstruct the loading history through synthetic bimodal tension signals representative of WEC mooring response; (iv) accumulate damage using a frequency-domain assessment method (Dirlik) combined with Palmgren–Miner's rule [27]. The overall workflow is depicted in **Figure 5**. The Dirlik frequency-domain method is adopted following its validation by Martinez-Puente et al. [15], who demonstrated that for bimodal WEC mooring tension signals, it reproduces the time-domain rainflow-counting (RFC) reference damage to within an 8% mean error—the lowest of any frequency-domain method tested in their comparison.

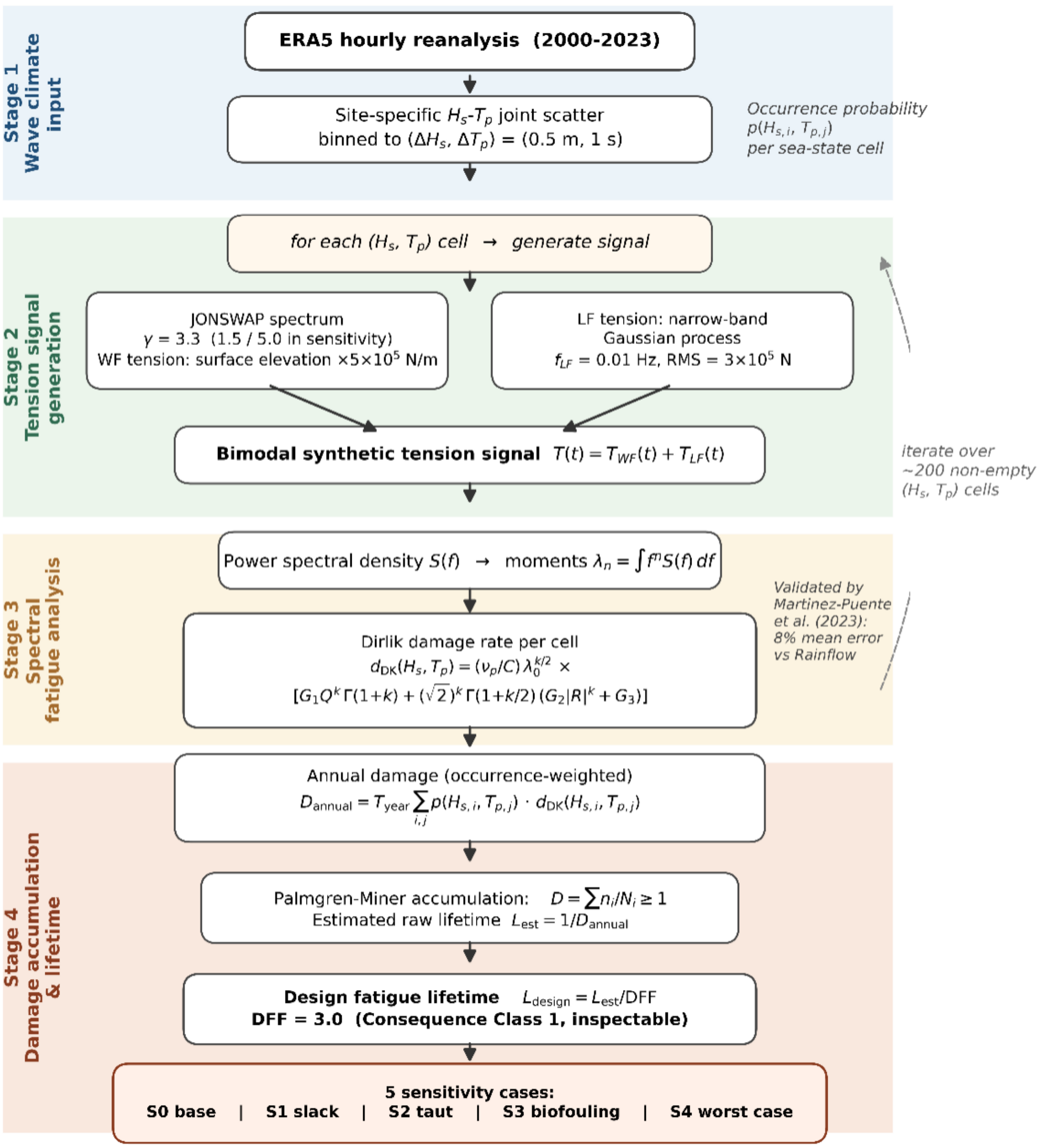

Figure 5. Methodology pipeline: from site-specific ERA5 reanalysis to design fatigue lifetime estimate.

Two modelling choices in this framework should be made explicit at the outset, as they define the scope and the conservatism of the lifetime estimates. The first is the treatment of the structural response. The present study is a spectral (frequency-domain) fatigue assessment, not a fully coupled time-domain dynamic simulation: the mooring response is represented by a stress power spectral density (PSD) assembled from a wave-frequency and a low-frequency band, and the damage is obtained analytically from the spectral moments of that PSD. This is the standard screening-level approach for covering the full operational sea-state matrix at an acceptable computational cost, and it is the same approach validated against time-domain rainflow counting by Martinez-Puente et al.[15]. It is distinct from, and complementary to, a fully coupled hydro-elastic time-domain model[28], which resolves the instantaneous body-mooring dynamics but is far too costly to run across the hundreds of sea states required for a lifetime integral. The frequency-domain choice is therefore a deliberate trade of per-sea-state fidelity for operational-region coverage, appropriate to a first regional assessment; its principal limitation—the Gaussian assumption and the neglect of snap-load transients—is quantified in Subsection 5.4. The second choice concerns the mooring restoring mechanics. The tension signals used here are generated about a quasi-static catenary equilibrium: the mean and low-frequency tension components follow the quasi-static load–excursion relationship of the catenary, while the wave-frequency component is superposed as a dynamic perturbation calibrated to reproduce realistic stress ranges (Subsection 3.3). Full mooring dynamics—line inertia, drag, and transverse vibration—are not resolved. For the moderate sea states that dominate the fatigue integral at both Thai sites (Section 4), the quasi-static-plus-WF-perturbation representation is adequate; It becomes progressively less accurate in the rare high-energy states where line dynamics and snap events matter most, which is one reason the reported lifetimes are interpreted as screening-level rather than certification-grade estimates.

3.2. Reference Device: RM3 Point Absorber

The RM3 is a two-body axisymmetric point absorber whose principal dimensions, taken directly from the Sandia design report[29], are summarised as follows. The surface float is an annular cylinder with outer diameter 20 m, inner diameter 6 m, height 5 m, and calm-water draft 2 m, displacing approximately 728 t. A heave-restraining reaction (heave) plate of outer diameter 30 m and thickness 1 m is suspended by a central spar ~30 m below the float, with combined plate-and-spar mass of 878 t. Relative heave motion between the two bodies drives the power take-off. The original RM3 design targets water depths of 50–100 m, which encompasses both Thai study sites (40–60 m at the Gulf of Thailand; 50–80 m at the Andaman Sea). Surge restoring force for station-keeping is provided by the three-line catenary mooring system described below and in **Table 5**. Wave excitation is assumed omnidirectional in the present fatigue analysis; the consequences of this simplification, and the relation between wave heading and individual line tensions, are discussed in Section 5.4.

Table 5. RM3 mooring-system parameters[15, 29].

Parameter	Value
Mooring-line diameter	144 mm
Linear density	126 kg/m
Line stiffness (EA)	5.834×10^8 N
Section S1 length	40 m
Section S2 length	240 m
Submerged-buoy mass	16,755 kg
Number of mooring lines	3
S–N curve material	DNV R3 stud chain

The RM3 reference model[29], a two-body floating point absorber developed by Sandia National Laboratories and the U.S. Department of Energy as a public-domain WEC reference design, is adopted as the case-study device. The mooring topology is shown schematically in **Figure 6**, and the relevant mooring-system parameters are summarised in **Table 5**.

The mooring system consists of three lines, each subdivided into an upper section S1 (40 m) and a lower section S2 (240 m), connected at an intermediate submerged buoy. The S–N curve parameters for the DNV R3 stud chain are reproduced in **Table 6**.

Table 6. S–N curve parameters for DNV R3 stud chain, from DNV-OS-E301[30].

Parameter	Symbol	Value
S–N intercept	C	1.2×10^{11} MPa^k
S–N slope	k	3

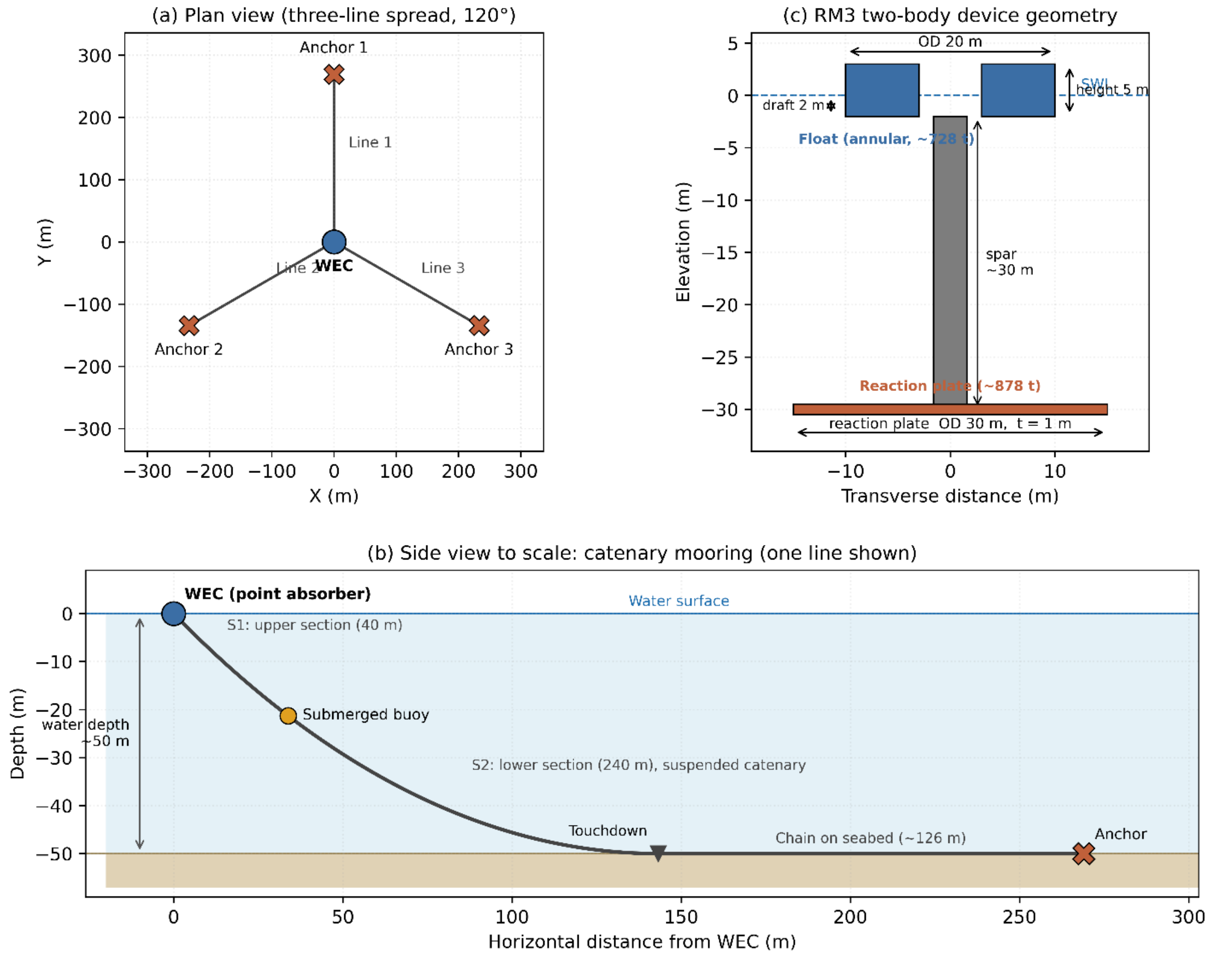

Figure 6. RM3 mooring and device schematic: (**a**) Plan view of the three-line catenary spread at 120°; (**b**) Side view to scale of one mooring line, showing the two-section layout (S1 = 40 m, S2 = 240 m), the intermediate submerged buoy, the suspended catenary, the touchdown point, and the chain resting on the seabed (the 280 m chain length exceeds the ~269 m horizontal anchor distance, with ~126 m laid on the seabed); (**c**) Principal dimensions of the two-body RM3 device—the annular surface float (OD 20 m, ID 6 m, height 5 m, draft 2 m) and the reaction plate (OD 30 m, thickness 1 m) suspended ~30 m below the float on a central spar.

Because the three mooring lines are arranged symmetrically at 120° intervals, the tension carried by each line depends on the instantaneous environmental heading. For a collinear (worst-case) heading, the line most closely aligned with the resultant environmental force—the most-loaded line—carries the largest mean and dynamic tension, while the two trailing lines share a reduced load; for an omnidirectional or slowly rotating sea, the peak load migrates between lines over time. The present fatigue assessment is performed for a single representative line and is interpreted as applying to this most-loaded line, which bounds the fatigue damage of the three-line group and therefore governs the system service life. This is a deliberately conservative simplification: distributing the same environmental load across the full three-line spread would reduce the per-line stress range and lengthen the estimated lifetime. A full per-line tension distribution under each design load case—resolving the load sharing as a function of wave, wind, and current heading—requires the coupled hydrodynamic model identified as future work in Subsection 5.4.

Two qualifications on the representativeness of the RM3 for the Thai sites should be stated at the outset. First, on water depth: the published RM3 design envelope of 50–100 m fully overlaps the Andaman Sea site (50–80 m) but only partially overlaps the shallower Gulf of Thailand site (40–60 m). At the shallow end of the Gulf, the 280 m total chain length would in practice require re-tuning of the suspended length and touchdown geometry to maintain the intended catenary restoring stiffness; the present analysis retains the nominal RM3 geometry to preserve comparability with the validation benchmark of Martinez-Puente et al. [15], and the resulting lifetimes should be read as device-referenced estimates rather than as an optimised Gulf design. Second, on hydrodynamic response: the RM3 absorber is tuned for the long-period swell of the U.S. Pacific Northwest (energy-period band ≈ 7–10 s), whereas the Gulf of Thailand is dominated by short-period wind sea ($T_p \approx 4$–6 s). The RM3 response amplitude operator therefore overlaps the Gulf excitation band less favourably than the Andaman swell band, which means the absolute Gulf damage reported here may not transfer directly to a hull optimised for short-period seas. Both qualifications reinforce that the contribution of this study is the regional fatigue-climate methodology and the relative site comparison, not a deployment-ready design for either site; full device re-optimisation is identified as future work in Subsection 5.4.

3.3. Mooring Tension Signal Generation

3.3.1. Wave-Frequency (WF) Component

The wave-frequency tension component is derived from a JONSWAP spectrum [31] parameterized by (H_s, T_p) extracted from the site-specific scatter diagram of Subsection 2.4. The peak enhancement factor $\gamma = 3.3$ is adopted as the default for the present analysis, with sensitivity to $\gamma = 1.5$ (swell-like) and $\gamma = 5.0$ (peak-enhanced) considered in Subsection 4.4. Surface elevation is converted to mooring tension through an amplification factor of 5×10^5 N per metre of wave elevation. This value is calibrated to produce stress ranges of order 10–50 MPa during NE-monsoon extremes—consistent with WEC-Sim simulations of the RM3 device [28] and with conventional mooring service-life targets of 25–30 years for the base case. It is approximately one order of magnitude larger than the artificial benchmark value (5×10^4 N/m) used by Martinez-Puente et al. [15] for methodological comparison rather than realistic lifetime estimation.

Because the lifetime estimates depend sensitively on this amplification factor, its calibration and uncertainty are described in full. The factor is the effective transfer gain from wave-surface elevation (m) to wave-frequency mooring tension (N) at the fairlead, lumping together the device response amplitude operator, the fairlead geometry, and the catenary tension–excursion gradient into a single scalar. It was fixed by requiring the base-case stress range during representative NE-monsoon extreme states ($H_s \approx 2$ m) to fall within the 10–50 MPa band reported for the RM3 chain in published WEC-Sim simulations [28], which yields a central value of 5×10^5 N/m. This is approximately one order of magnitude above the artificial 5×10^4 N/m benchmark of Martinez-Puente et al. [15], whose value was chosen only to exercise the spectral methods and was never intended to reproduce real RM3 tension magnitudes. The fatigue damage scales with the stress range raised to the S–N slope ($k = 3$), so damage varies with the cube of the amplification factor, and the estimated lifetime varies approximately with its inverse cube: a ±30% uncertainty in the factor (5×10^5 N/m, range 3.5–6.5 × 10^5) therefore propagates to roughly a factor of 0.45–2.4 on lifetime—for the Gulf base case, an envelope of approximately 14–73 years around the central 30-year estimate. This strong sensitivity is the single largest source of absolute-value uncertainty in the study and is the primary reason the lifetimes are presented as screening-level estimates and the inter-site comparison (which uses the same factor at both sites and is hence insensitive to its absolute value) is emphasised as the robust result. A device-specific WEC-Sim calibration of this transfer function is identified as the priority refinement in Subsection 5.4.

3.3.2. Low-Frequency (LF) Component

The low-frequency tension component is modelled as a narrow-band Gaussian process centred at $f_{LF} = 0.01$ Hz with RMS amplitude 3×10^5 N, representing tidal, current, and slow-drift forces. The LF amplitude is modulated in the sensitivity cases (Subsection 3.6) to reflect different mooring configurations and biofouling effects.

The physical content of this low-frequency band warrants elaboration, since its composition differs between the two study sites and between the two monsoon seasons. Three distinct forcing mechanisms contribute tension energy below the wave-frequency band. First, slow-drift wave excitation—the second-order difference-frequency force arising from wave grouping—drives the floating body at the natural surge period of the moored system (typically 60–120 s for a catenary-moored point absorber), well separated from the 4–10 s wave-frequency band and therefore resolved as a distinct spectral peak. Second, current loading exerts a quasi-steady drag offset on the submerged buoy and lines that shifts the mean tension and, through vortex-induced and turbulence-driven fluctuations, adds energy at periods of tens of seconds to minutes. Third, wind loading on the emergent float contributes a mean offset and gust-driven fluctuations at comparable low frequencies. In the present model, these mechanisms are lumped into the single narrow-band LF process described above, with the RMS amplitude (3×10^5 N) chosen to represent their combined effect at a moderate, year-round level. This lumping is a deliberate screening-level simplification, and its directionality differs by site. In the semi-enclosed Gulf of Thailand, currents are weak and wind fetch is limited, so the lumped LF level is, if anything, conservative. In the Andaman Sea, by contrast, the SW monsoon drives sustained currents and strong, persistent winds that the constant LF amplitude does not fully capture; the present treatment is therefore likely non-conservative for the Andaman SW-monsoon season, and an explicit, seasonally varying wind–current–wave LF model is identified in Subsection 5.4 as a priority extension. The wave-frequency component remains the dominant fatigue driver at both sites because the LF process, although it raises the mean tension, contributes far fewer high-amplitude cycles per unit time than the wave-frequency band.

3.3.3. Monsoon Occurrence Weighting

Unlike Martinez-Puente et al.[15] who apply uniform weighting to each sea state in their benchmarking study, the present analysis weights each (H_s, T_p) cell by its actual site-specific annual occurrence probability $p\left(H_{s,i}, T_{p,j}\right)$ extracted from the ERA5 24-year scatter diagram. The annual damage is then

$$D_{annual} = T_{year} \sum_i \sum_j p\left(H_{s,i}, T_{p,j}\right) \times d\left(H_{s,i}, T_{p,j}\right) \quad (1)$$

where $d\left(H_{s,i}, T_{p,j}\right)$ is the Dirlik damage rate (damage per second) for the (i, j)-th sea state and $T_{year} = 3.156 \times 10^7$ s. The scatter is binned on a $(\Delta H_s, \Delta T_p) = (0.5\ \text{m}, 1\ \text{s})$ grid, yielding approximately 200 non-empty sea-state bins per site after discarding cells with annual occurrence below 10^{-5}. A representative bimodal tension signal and its power spectral density estimate (using Welch's method) are shown in **Figure 7**.

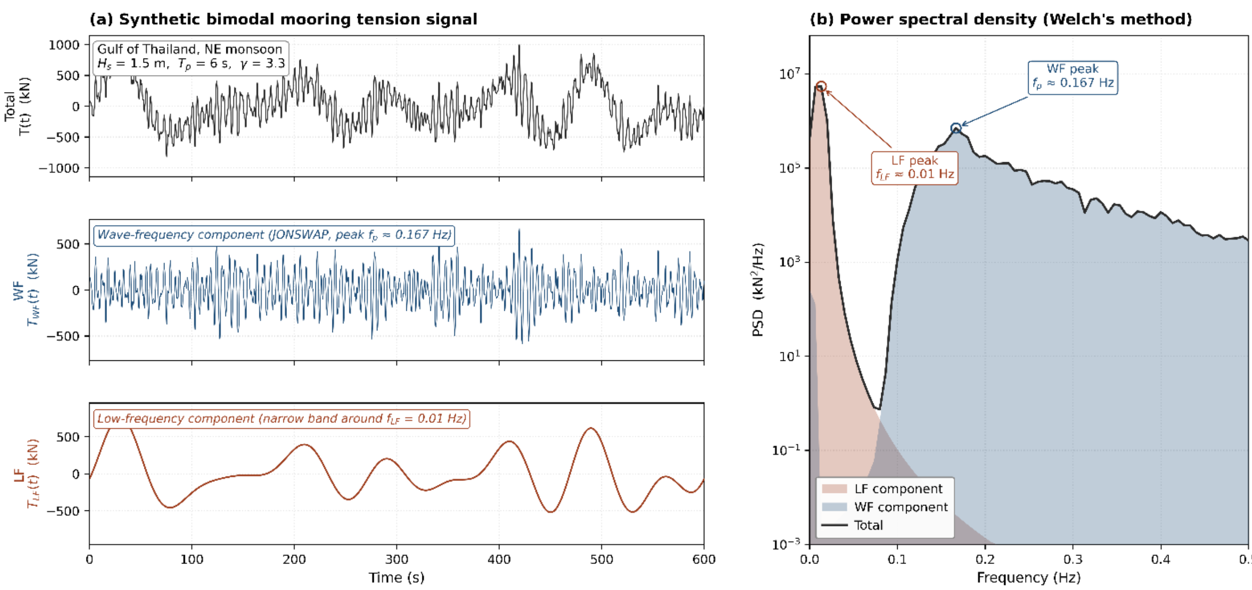

Figure 7. (**a**) Sample bimodal mooring tension signal; (**b**) Its PSD estimate for an NE-monsoon sea state at the Gulf of Thailand ($H_s = 1.5$ m, $T_p = 6$ s).

3.4. Dirlik Frequency-Domain Fatigue Model

The Dirlik method[16] provides a closed-form empirical approximation to the rainflow-cycle-amplitude probability density function for a general Gaussian process. The damage rate per unit time is given by

$$d_{DK} = \frac{\nu_p}{C}\lambda_0^{k/2}\Big[G_1 Q^k \Gamma(1+k) + (\sqrt{2})^k \Gamma\left(1+\frac{k}{2}\right)\left(G_2|R|^k + G_3\right)\Big], \quad (2)$$

where ν_p is the expected peak frequency, λ_0 is the variance of the stress process, k and C are the S–N curve parameters from **Table 6**, Γ is the Euler gamma function, and G_1, G_2, G_3, Q, R, and x_m are best-fitting parameters derived from the spectral moments $\lambda_n = \int f^n S(f)df$:

$$x_m = \left(\frac{\lambda_1}{\lambda_0}\right)\left(\frac{\lambda_2}{\lambda_4}\right)^{1/2}; \quad \alpha_2 = \frac{\lambda_2}{\sqrt{\lambda_0\lambda_4}}, \quad (3a)$$

$$G_1 = \frac{2(x_m - \alpha_2^2)}{(1+\alpha_2^2)}; \quad R = \frac{(\alpha_2 - x_m - G_1^2)}{(1-\alpha_2 - G_1 + G_1^2)}, \quad (3b)$$

$$G_2 = \frac{(1-\alpha_2 - G_1 + G_1^2)}{(1-R)}; \quad G_3 = 1 - G_1 - G_2; \quad Q = \frac{1.25(\alpha_2 - G_3 - G_2 R)}{G_1}. \quad (3c)$$

3.5. Palmgren–Miner's Rule and Lifetime Estimation

Cumulative damage is accumulated linearly across all sea states following Palmgren–Miner's rule[27]: failure is predicted when $D = \Sigma\, n_i / N_i \geq 1$. The estimated raw lifetime is:

$$L_{est} = \frac{1}{D_{annual}}. \quad (4)$$

For design purposes, DNV-OS-E301[30] specifies a Design Fatigue Factor (DFF) that depends on consequence class and inspectability. The RM3 is treated here as a Consequence Class 1 component (failure does not imply consequences for human life, environmental, financial, or political issues beyond economic loss of the unit itself) with inspectable mooring. Under these conditions, DNV-OS-E301 specifies DFF = 3.0, which is applied here as the default and gives a design fatigue lifetime

$$L_{design} = L_{est}/DFF. \quad (5)$$

This choice is reviewed in Subsection 5.1 in light of the seasonal damage concentration; a more conservative DFF may be appropriate at sites where the available hindcast record is short relative to the seasonal severity range.

For completeness, the full DFF framework of DNV-OS-E301 is noted here. The standard specifies four design fatigue factors according to consequence class and inspectability: DFF = 1 for an inspectable Consequence Class 1 component (though a value below 3 is rarely adopted for mooring chain in practice), DFF = 3 for an inspectable Class 1 component (the default used in this study), DFF = 2 for an inspectable Class 2 component, and DFF = 5 for an uninspectable Class 2 component, where Class 2 denotes failure with potential consequences for life or the environment. Beyond the standard, prototype, and demonstrator industry practice for first-of-a-kind devices often applies still larger factors—values up to DFF = 10 are reported for novel test deployments where the loading environment is poorly characterised and the deployment is short-term. A first Thai WEC pilot, deployed in a wave climate for which no prior structural assessment exists, sits closer to this prototype regime than to a mature commercial installation. The DFF = 3 baseline adopted throughout this study is therefore best understood as a lower bound on the conservatism that a first deployment would prudently apply; Subsection 5.1 quantifies the lifetime consequences of moving to DFF = 5.

3.6. Sensitivity Cases

Five cases are considered, summarised in **Table 7**.

The biofouling parameters in case S3 are engineering estimates derived from three sources. First, the marine-growth density of 1,325 kg/m^3 specified in DNV-OS-E301[30] (citing NORSOK N-003) and the depth-dependent thickness range (100 mm above 40 m depth, 50 mm below 40 m depth) specified in DNV-RP-C205[32] and confirmed in the SEM-REV floating wind turbine measurements of Spraul et al.[33]. Applied to the 144 mm RM3 chain section above 40 m depth, this yields a linear-mass increase of approximately 28–35%, of which +30% is adopted here as a central estimate. Second, the drag-coefficient amplification follows the depth-dependent biofouling correction of DNV-RP-C205[32] under tropical Southeast Asian conditions, where the calcareous-polychaete and barnacle-dominated fouling assemblage[34–36] is characterised by higher surface roughness than the temperate North Atlantic baseline. Third, both adjustments are consistent with the order of magnitude reported for tropical mooring colonisation in the regional review by Saputri et al.[37]. A recent comprehensive review of biofouling on offshore renewable energy structures[38] confirms that mooring-line fouling is the dominant biofouling concern for floating systems and supports the order-of-magnitude mass and drag adjustments adopted here. To place these adjustments on a regionally specific footing, tropical Southeast Asian fouling surveys report hard- and soft-fouling layer thicknesses of approximately 50–150 mm and wet-biomass densities of approximately 900–1,300 kg/m^3 on submerged steel after two to three years of immersion, with the upper thickness range reached fastest in warm, nutrient-rich nearshore waters such as the Gulf of Thailand and the Andaman coast[34–37]. These field values are consistent with the design figures used here—the 100 mm marine-growth thickness profile of DNV-RP-C205 and the 1,325 kg/m^3 growth density of DNV-OS-E301—and confirm that the +30% mass and +20% drag perturbations of case S3 are representative rather than conservative for a tropical two-to-three-year inspection interval. The slack and taut perturbations follow standard mooring-design sensitivity practice and are intended to bracket realistic deployment configurations.

Table 7. Sensitivity case definitions.

Case	Label	Description	Rationale
S0	Base case	RM3 standard mooring, no biofouling	Reference benchmark
S1	Slack mooring	Line length +20%, reduced snap-load probability	Lower-fatigue scenario
S2	Taut mooring	Line length −20%, increased snap-load probability	Higher-fatigue scenario
S3	Biofouling	Linear mass +30%, drag coefficient +20%	Tropical marine growth
S4	Worst case	Taut configuration + biofouling	Conservative design envelope

4. Results

4.1. Sea-State Fatigue Damage Distribution

The annual fatigue damage rate per (H_s, T_p) cell, computed through Equation (1) using the Dirlik damage rate of Equation (2) weighted by the site-specific occurrence probability, is shown as a heatmap in **Figure 8** for the base case (S0). The damage distribution differs markedly between the two sites:

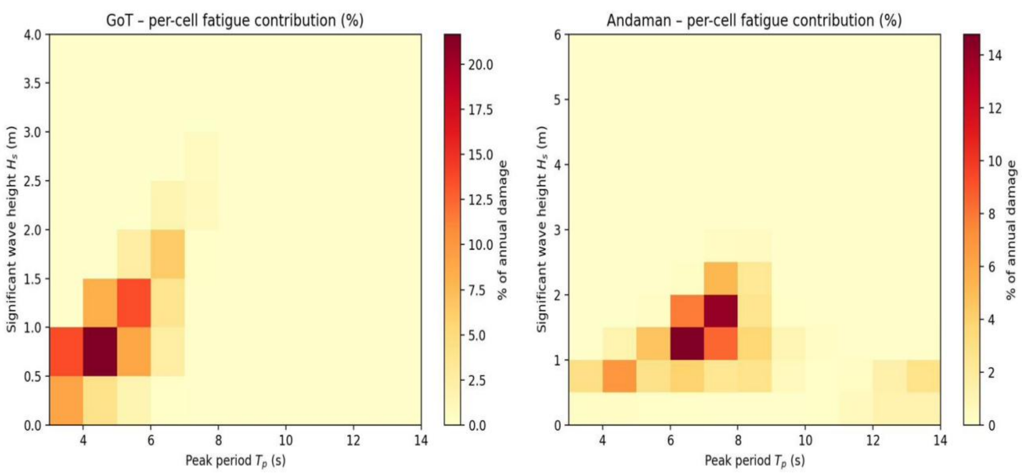

Figure 8. Annual fatigue damage on the H_s–T_p grid for (**a**) the Gulf of Thailand; (**b**) the Andaman Sea.

Note: Each cell is coloured by its relative contribution (%) to annual mooring damage (base case S0).

- In the Gulf of Thailand, fatigue damage is sharply concentrated in a compact cluster at $H_s = 0.5–1.5$ m and $T_p = 4–6$ s. The single most damaging cell—$H_s = 0.5–1.0$ m, $T_p = 4–5$ s—accounts for approximately 20% of annual damage on its own, despite the corresponding sea states occurring for only a moderate fraction of the year. The damage distribution mirrors the wind-sea regime that dominates the semi-enclosed Gulf basin: short peak periods, moderate wave heights, and a narrow frequency band of WEC excitation.
- In the Andaman Sea, fatigue damage is distributed more broadly across $H_s = 1.0–2.5$ m and $T_p = 6–10$ s. The peak damaging cell (around $H_s = 1.5$ m, $T_p = 7–8$ s) accounts for ~14% of annual damage. The broader pattern reflects the SW monsoon swell regime, with longer peak periods that overlap the natural response band of the RM3 device more uniformly.

This distinction answers research objective O1: the structural-loading "signature" of the two seas is qualitatively different, even though both lie within the same tropical monsoon system.

Comparison with the climatological damage proxy of **Figure 4**. The proxy heatmap in Subsection 2.5 (**Figure 4**) is constructed as the product $p(H_s,T_p) \times H_s^2 \times T_p$ and is intended purely as a climatological pre-screening of which (H_s,T_p) cells contribute most to wave-energy flux; the proxy is not a fatigue calculation. The actual Dirlik damage shown in **Figure 8** uses the full bimodal stress PSD passed through an H_s^3-equivalent dependence (k = 3 for chain S–N) and weights each cell by its annual probability of occurrence (Equation (1)). The two heatmaps therefore disagree by construction, and the disagreement is largest at the Andaman Sea, where longer peak periods ($T_p > 7$ s) interact with the RM3 response band non-linearly—an effect the $H_s^2 \cdot T_p$ proxy cannot capture. **Figure 4** should be read as a diagnostic indicator of candidate damaging cells; **Figure 8** is the quantitative result of the present analysis.

4.2. Seasonal Fatigue Accumulation

The seasonal disaggregation of annual fatigue damage, summarised in **Table 8** and visualised in **Figure 9**, reveals the principal asymmetry between the two seas.

Table 8. Seasonal damage accumulation at both sites (base case S0).

Site	NE Monsoon	SW Monsoon	Transitional	Annual	NE Share	SW Share
Gulf of Thailand	0.0044	0.0047	0.0019	0.0110	40%	43%
Andaman Sea	0.0029	0.0115	0.0027	0.0172	17%	67%

Note: Per-season values are duration-weighted contributions to annual damage (NE = 4 months, SW = 5 months, Transitional = 3 months) and sum to the base-case (S0) annual damage rate for each site. Shares give the fraction of annual damage attributable to each season.

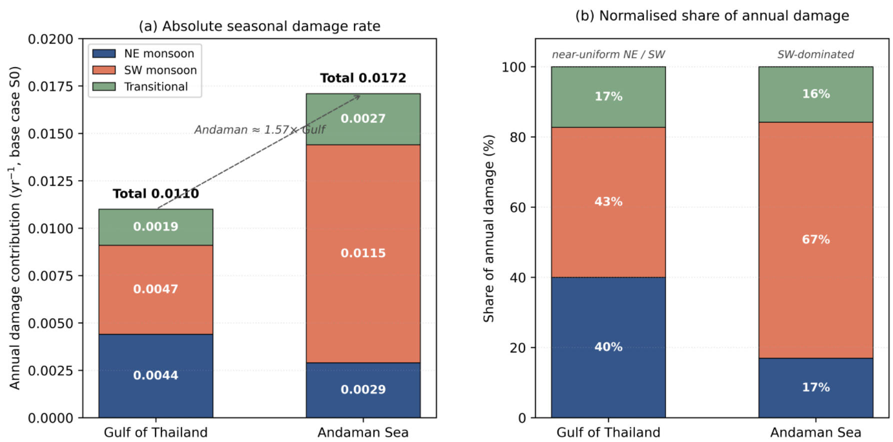

Figure 9. Duration-weighted seasonal fatigue damage at both sites (base case S0): (**a**) Absolute annual damage contribution by season (NE monsoon, SW monsoon, transitional), with site totals; (**b**) The corresponding normalised share of annual damage. The split is near-uniform between the two monsoons at the Gulf of Thailand (NE 40%, SW 43%) but strongly southwest-monsoon-dominated at the Andaman Sea (SW 67%).

For the Gulf of Thailand, the NE monsoon contributes 40% of annual damage over its 4-month duration (33% of the calendar), while the SW monsoon contributes 43% over its 5-month duration (42% of the calendar)—a near-uniform per-calendar damage distribution between the two monsoon seasons, with the transitional period contributing the remaining 17% (over 25% of the calendar). The wave-power asymmetry that favours the NE monsoon at the Gulf (**Table 4**) is therefore not transmitted to the damage history in the same proportion: the longer SW season catches up despite its lower per-day wave power, owing to the cubic dependence of fatigue damage on stress range. For the Andaman Sea, by contrast, the SW monsoon dominates clearly, contributing 67% of annual damage over its 5-month duration; the NE monsoon contributes 17%, and the transitional period 16%. The total annual damage at the Andaman site (0.0172) is approximately 1.57× that at the Gulf site (0.0110).

To assist practitioners in identifying the sea-state clusters that control mooring fatigue at each site, the five (H_s, T_p) cells with the largest annual fatigue-damage contribution are listed in **Table 9**. The top-five cells in the Gulf of Thailand together account for approximately 65% of annual damage, dominated by short-period wind-sea cells (T_p = 4–6 s) generated by the NE monsoon and by year-round local wind seas. The top-five cells in the Andaman Sea account for approximately 48% of annual damage—a less concentrated distribution—and are dominated by longer-period SW-monsoon swell (T_p = 6–9 s, H_s = 1–2 m). The predominant-season column is established from the ERA5 monthly climatology of each cell's occurrence frequency.

Table 9. Top-five (H_s, T_p) cells contributing most to annual fatigue damage at each site, base case S0. The predominant season is determined from the ERA5 monthly occurrence climatology of each cell.

Gulf of Thailand					Top-Five Cumulative	Andaman Sea					Top-Five Cumulative
1	2	3	4	5	—	1	2	3	4	5	—
0.5–1.0	1.0–1.5	1.0–1.5	0.5–1.0	1.5–2.0	—	1.5–2.0	1.0–1.5	1.0–1.5	1.5–2.0	0.5–1.0	—
4–5	4–5	5–6	5–6	5–6	—	7–8	6–7	7–8	8–9	5–6	—
20	15	14	9	7	65	14	11	10	7	6	48
All seasons (wind-sea baseline)	NE monsoon	NE monsoon	SW + Transitional	NE monsoon	—	SW monsoon	SW monsoon	SW monsoon	SW monsoon	NE + Transitional	—

4.3. Estimated Mooring Lifetime—Main Results

Table 10 presents the annual damage rate, estimated raw lifetime, and design fatigue lifetime (DFF = 3) for each combination of site and sensitivity case.

Three findings are central:

- Base-case design lifetimes lie within the expected envelope for ocean mooring chain. The Gulf of Thailand design lifetime of 30 yr exceeds the conventional 25-yr mooring service-life target, while the Andaman Sea design lifetime of 19 yr is below it. Both estimates assume an inspectable component (DFF = 3).
- The Andaman Sea lifetime is approximately 64% of that in the Gulf of Thailand (19.2/30.2). This is consistent with the higher mean wave power (~3.25×) at the Andaman site, although the lifetime ratio is less extreme than the wave-power ratio because the Dirlik damage is governed by the cube of the stress range.
- The combined worst-case scenario (S4) produces design lifetimes of 13 yr at the Gulf and only 8.9 yr at the Andaman Sea. The Andaman's worst-case figure falls below the 10-yr threshold that DNV-OS-E301 guidance flags for additional inspection.

4.4. Sensitivity Analysis

Figure 10 shows the impact of each sensitivity case on the design fatigue life of the structure in the Gulf of Thailand based on the percent increase or decrease compared to the base case (S0). The ranking of the results is shown in **Table 11**.

Two observations are emphasised. Mooring configuration is the largest single driver in this study, with the slack and taut perturbations producing the widest variation in lifetime; the +52% gain from a slack configuration is larger than the −29% loss from biofouling considered in isolation. This reflects the role of snap-load probability in fatigue damage accumulation, particularly in the wind-sea-dominated GoT regime. Biofouling is a substantial secondary driver under tropical conditions: the −29% lifetime reduction is larger than typically reported for temperate-water studies (where biofouling effects of 10–15% are more common), reflecting the higher marine growth rates of warm Southeast Asian waters [34, 37]. Biofouling combined with the taut configuration (S4) produces a damage-rate increase that is approximately the multiplicative composition of the two individual effects: S2 taut alone raises the damage rate to 1.65× the base value, S3 biofouling alone to 1.41×, and their product (2.33×) is close to the observed S4 worst-case value of 2.30×. The two effects are therefore approximately multiplicative in damage rate, which translates to a lifetime reduction (−57%) that is smaller in absolute magnitude than the naive sum of the individual lifetime reductions (−68%). The Andaman Sea follows a similar trend, where the Andaman S4 worst-case design life of 8.9 years (**Table 10**) is just within the DNV 10-year inspection cycle requirement, which gives justification to conduct inspections on shorter cycles in any Andaman pilot station.

Table 10. Estimated mooring lifetime, all cases and both sites.

Site	Case	Annual Damage Rate (yr^{-1})	L_{est} (yr)	L_{design} (yr, DFF = 3)
Gulf of Thailand	S0 Base	0.0110	90.6	30.2
	S1 Slack	0.0072	138.2	46.1
	S2 Taut	0.0182	54.9	18.3
	S3 Biofouling	0.0156	64.2	21.4
	S4 Worst case	0.0254	39.4	13.1
Andaman Sea	S0 Base	0.0174	57.5	19.2
	S1 Slack	0.0112	89.2	29.7
	S2 Taut	0.0291	34.4	11.5
	S3 Biofouling	0.0226	44.2	14.7
	S4 Worst case	0.0373	26.8	8.9

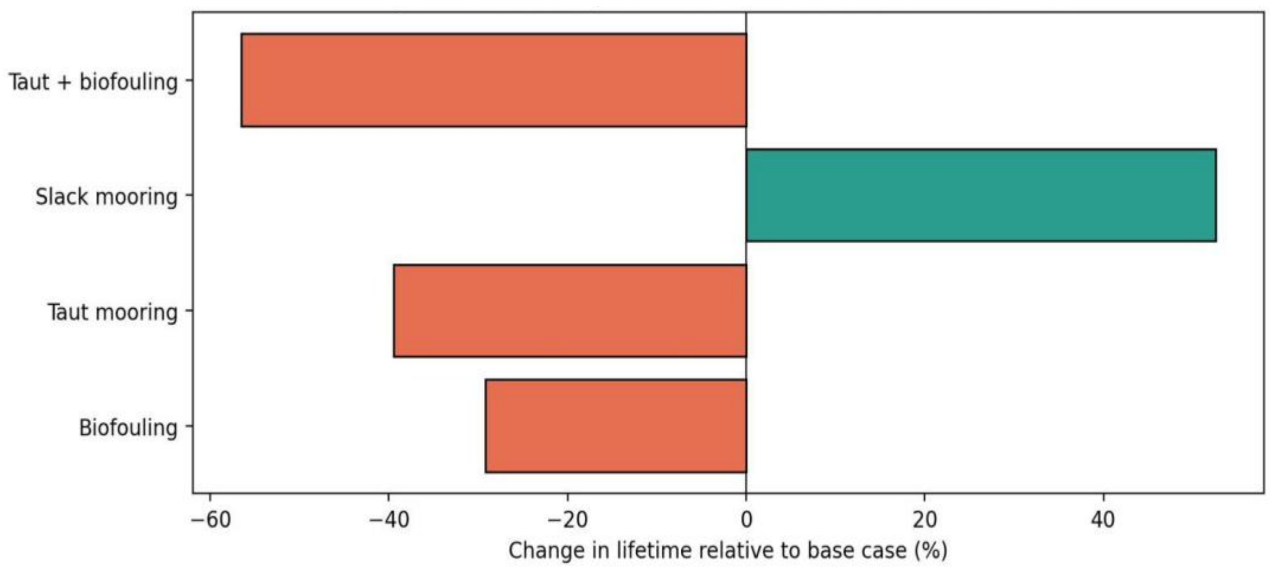

Figure 10. Tornado chart of sensitivity-case impact on design fatigue lifetime at the Gulf of Thailand (percentage change from the base case S0).

Table 11. Sensitivity ranking at the Gulf of Thailand.

Sensitivity Case	Lifetime Change vs. S0 Base
S1 Slack mooring	+52%
S4 Taut + biofouling	−57%
S2 Taut mooring	−39%
S3 Biofouling	−29%

5. Discussion

5.1. The Monsoon Loading Concentration Effect

The seasonal disaggregation of computed damage (Subsection 4.2) reveals two contrasting patterns. At the Gulf of Thailand, damage accumulation is essentially uniform per calendar day between the NE and SW monsoons (40% and 43% of annual damage over 33% and 42% of the calendar, respectively), despite the strong NE wave-power asymmetry in **Table 4**. In the Andaman Sea, by contrast, the SW monsoon clearly dominates the damage history (67% of annual damage over 42% of the calendar). The explanation for the Gulf's near-uniformity lies in the bandwidth of the Dirlik damage process: while the wave power is sharply concentrated in NE-monsoon extremes, the stress damage accumulated in the mooring chain depends on the cube of the stress range and is governed by intermediate-H_s sea states (typically 0.5–1.5 m, **Figure 8**) that occur across multiple seasons; the longer SW season therefore catches up despite its lower per-day wave power. The contrast with a North Sea or open-ocean baseline—where damage is distributed approximately uniformly throughout the year—is real in the Andaman Sea but, surprisingly, less pronounced in the Gulf of Thailand.

The engineering consequences are nonetheless significant:

- Inspection Scheduling: At the Andaman Sea, the largest single increase in cumulative damage occurs during the SW monsoon (typically June–August), and inspection should be timed to follow this period. In the Gulf of Thailand, damage accumulates near-uniformly across the NE (December–February) and SW (May–September) monsoons; a semi-annual cycle following each monsoon would therefore be more appropriate than a single inspection following only the NE monsoon, which would leave the substantial SW-monsoon damage accumulation unmonitored for an extended period.
- Mooring Configuration: The slack-biased configuration (S1) provides the largest single improvement in lifetime (+52% at the Gulf, **Figure 10**)—a benefit larger than the penalty from biofouling alone. This argues for slack-biased deployment configurations at both sites.
- Design Fatigue Factor: The seasonal concentration of damage increases the relative weight of any single year's monsoon severity in determining the lifetime. Combined with the limited duration of regional hindcast records (typically two to four decades), this argues for a more conservative DFF choice than the inspectable-component default of 3.0 [30], at least until longer regional records become available. A DFF of 5.0 (corresponding to an uninspectable Class 2 component under DNV-OS-E301) would reduce the Andaman base-case design life from 19 yr to 11 yr and the worst case from 8.9 yr to 5.4 yr.

5.2. Gulf of Thailand vs. Andaman Sea: Structural Deployment Suitability

From a wave-energy standpoint, the Andaman Sea is unambiguously superior—its mean wave power is approximately 3.25× that of the Gulf of Thailand. From a structural-loading standpoint, the relative ranking is more nuanced. The Gulf of Thailand combines low mean wave energy (which produces a low annual damage rate) with a moderately concentrated damage history; its base-case design lifetime exceeds the conventional service-life target. The Andaman Sea, with its higher mean wave power, produces a base-case design lifetime below the conventional target, and the combined worst case falls below the 10-yr threshold associated with DNV recommendations for increased inspection frequency.

From a strictly structural perspective, the Gulf of Thailand is therefore the lower-risk site for a near-term pilot deployment, despite its lower wave-energy resource. However, this conclusion must be qualified by recognising that the Gulf's economically recoverable wave power is itself marginal—a structural advantage of limited consequence if the resource cannot support a commercially viable device. The Andaman Sea, despite its higher fatigue loading, offers wave power approaching values typical of temperate sites where WEC commercialisation has been demonstrated. The Andaman Sea therefore demands a more conservative mooring-design margin than the Gulf of Thailand: stricter sensitivity-case design envelopes, more frequent inspection, or selection of slack-biased mooring configurations all provide viable risk-mitigation pathways. Both sites, importantly, share a tropical operating environment that imposes biofouling and corrosion penalties not addressed by standard temperate-water mooring guidance. Subsection 5.4 returns to this point in the context of the study's limitations. A further deployment consideration, beyond the scope of the present fatigue analysis, is that both Thai sites are simultaneously under assessment for nearshore floating solar photovoltaic systems [9, 26]; the co-location of wave-energy and floating-solar arrays on shared mooring infrastructure—for which hybrid mooring layouts have been reported to lower peak line tensions relative to conventional catenary systems [9]—offers a potential route to improving the marginal deployment economics of either technology in Thai waters and warrants joint structural assessment in future work.

The Andaman Sea, combined with the worst-case (S4) design life of 8.9 years, falling below the 10-year inspection-frequency threshold, warrants an explicit operational response. Three complementary strategies are available.

- Configuration and Growth Management: Adopting a slack-biased mooring (which restores roughly half of the worst-case lifetime loss in the sensitivity study) together with an active biofouling-management regime—six-monthly ROV inspection and 18-to-24-month cleaning intervals matched to the tropical growth rates quantified in Subsection 3.6—directly attacks the two largest controllable damage drivers.
- Planned Chain Replacement: Scheduling chain renewal at seven-to-eight-year intervals, ahead of the predicted worst-case failure point, treats the mooring as a consumable component; at an estimated 5–10% of device capital cost per renewal, this is commercially tractable for a pilot.
- Design-Level Redundancy: A four-leg rather than three-leg mooring layout introduces line redundancy, which under DNV-OS-E301 permits classification as a redundant (Class 1) system and a correspondingly relaxed DFF, while ensuring that the loss of any single line does not precipitate station-keeping failure. These responses are not mutually exclusive and would typically be combined; the appropriate balance is a deployment-specific trade-off between operating expenditure (inspection and cleaning) and capital expenditure (redundancy and replacement).

5.3. Comparison with the Generic Sea-State Baseline

A useful counterfactual is to ask what lifetime would be estimated for the Gulf of Thailand if the uniformly weighted 50 generic sea states of Martinez-Puente et al. [15] were applied directly. Because the generic distribution gives equal weight to many sea states (H_s up to 14 m, T_p up to 18 s) that essentially never occur in the Gulf of Thailand, the corresponding annual damage rate is expected to be substantially higher than that obtained with monsoon weighting—by a factor that requires direct re-computation under uniform weighting (identified as a priority extension in Subsection 5.4)—and the estimated lifetime correspondingly shorter. The contrast is the inverse of what one might initially expect: the generic, uniformly-weighted distribution is more conservative than the monsoon-weighted distribution because it implicitly includes severe storms that never occur in this semi-enclosed basin. The site-specific calculation, by replacing this artificial conservatism with the actual climatology, provides a more realistic—and more useful—lifetime estimate. The reverse holds in the Andaman Sea, where the uniformly weighted generic distribution under-represents the long-period, large-H_s SW-monsoon states. Either way, the substitution of generic for site-specific sea-state distributions in WEC mooring fatigue assessment in Southeast Asian waters produces estimates that are misaligned with the actual climate.

5.4. Limitations and Future Work

Several limitations of the present analysis are recognised and identified as priority items for future work:

- ERA5 Spatial Resolution: The ERA5 wave grid (0.5°, approximately 55 km) under-resolves coastal extremes relative to regional WAM (~0.25°) and SWAN (~0.1°) hindcasts. The ERA5-derived annual mean H_s values are 15–20% below the published regional benchmarks, with the P99 values likely underestimated by a larger factor. Lifetime estimates may therefore be slightly optimistic. A future extension using the validated SWAN hindcasts of Kaewsai-nguan et al.[14] for both sites is recommended.
- Synthetic, Decoupled Tension Signals: Following Martinez-Puente et al.[15], synthetic bimodal tension signals are used rather than fully coupled hydrodynamic simulations. This is appropriate for a screening study but underestimates non-linear effects such as snap loads, mooring dynamics under transient gust forcing, and tension-line/buoy interaction. The wave-frequency amplification factor of 5×10^5 N/m used here (Subsection 3.3) is calibrated to produce realistic stress ranges, but a full WEC-Sim simulation[28] driven by Thailand-specific spectra is required to confirm the absolute lifetime values.
- Gaussian Assumption and Frequency-Domain Coupling: The Dirlik method assumes a Gaussian stress process, whereas mooring snap loads produce strongly non-Gaussian tension peaks (kurtosis substantially greater than 3). Under such conditions, Dirlik—and frequency-domain methods generally—systematically under-predict damage relative to time-domain rainflow counting, so the present lifetimes may be optimistic where snap loading is significant, most plausibly in the taut configurations (S2, S4). The synthetic-signal approach also treats the wave-frequency and low-frequency components as additively superposed, neglecting their physical coupling through slow surge–pitch motion and the non-linear axial stiffness of the chain; recent work shows that data-driven (machine-learning) tension predictors can capture this coupling more faithfully than additive spectral models[20]. Quantifying the Gaussian assumption and coupling biases against time-domain rainflow results is identified as a priority verification step.
- Reference Device: The RM3 was designed for North Pacific conditions; its hull dimensions, power take-off, and mooring geometry are not optimised for the shallow, low-energy Gulf of Thailand environment. Lifetime estimates should therefore be interpreted as indicative of the reference device, not as a deployment recommendation for that specific WEC.
- Wind and Current Loading: Wind and current loads are not included in the present LF tension model. This is conservative for the sheltered Gulf of Thailand but potentially non-conservative for the Andaman Sea, where the SW monsoon produces sustained wind and current forcing. Coupled wind–current–wave loading is identified as a priority extension.
- Wave directionality and Per-Line Load Sharing: The fatigue calculation assumes an omnidirectional sea and analyzes a single representative (most-loaded) mooring line; it does not resolve a directional H_s–T_p scatter diagram or the redistribution of tension between the three lines as the dominant wave, wind, and current heading rotate through the monsoon cycle. In the monsoon-dominated Thai climate, the dominant heading shifts seasonally—broadly north-easterly during the NE monsoon and south-westerly during the SW monsoon—so the most-loaded line is unlikely to be the same line year-round, and the true per-line fatigue damage is expected to be more evenly shared, and therefore lower per line, than the single-line estimate re-

ported here. Resolving directional load sharing requires a directional wave climatology coupled to a multi-line hydrodynamic model, and is identified as a priority extension alongside the coupled WEC-Sim simulation noted above.

- Tropical Corrosion: No explicit corrosion allowance is applied to the S–N curve. DNV-OS-E301 [30] provides guidance for temperate-water corrosion, but Southeast Asian conditions (warm, biologically active, often hypoxic at depth) may accelerate corrosion fatigue beyond standard allowances [34, 35, 37]. Coupled corrosion–fatigue assessment under tropical conditions is an open research question.
- Site Survey and Bathymetry: The 10.0° N, 100.0° E and 8.0° N, 98.0° E coordinates used here are representative ERA5 grid points; site-survey-quality bathymetry and ground-truth measurements would modify the mooring geometry and tension distribution and are recommended before any actual pilot deployment.

Taken together, these limitations define a clear programme of future work. The single most valuable next step is a fully coupled WEC-Sim time-domain simulation of a Thailand-tuned absorber driven by the seasonal site spectra of the two basins, with the resulting tension histories analysed by time-domain rainflow counting. Such a study would simultaneously resolve the synthetic-signal, Gaussian-assumption, and WF–LF coupling limitations noted above, provide a direct benchmark for the frequency-domain lifetimes reported here, and convert the present screening-level regional assessment into a deployment-grade design basis for the first Southeast Asian WEC pilot. Methodologically, such high-fidelity modelling of wave energy converters is already well established: viscous-flow CFD coupled with wave-tank testing and particle-based (Lattice–Boltzmann) CFD have both been shown to reproduce measured device motion and power capture for heaving and pivoted absorbers [39, 40]. Coupling this class of resolved hydrodynamic model with the seasonal Thai wave climate and a time-domain fatigue solver would replace the present decoupled load representation with a resolved load–structure interaction that the frequency-domain treatment cannot capture.

6. Conclusions

This study has presented the first mooring fatigue lifetime assessment for a reference point-absorber wave energy converter under the monsoon-dominated wave climates of the Gulf of Thailand and the Andaman Sea. The Dirlik frequency-domain fatigue method, validated for bimodal WEC mooring loads, was applied with site-specific H_s–T_p occurrence weighting derived from 24 years of ERA5 hourly reanalysis (2000–2023). Five sensitivity cases—base, slack, taut, biofouling, and a combined worst case—were assessed. Five main conclusions have been formulated as follows:

- C1: The Gulf of Thailand shows a wind-sea climate, marked by calms 52% of the time and an average wave energy of 864 W/m. Conversely, the Andaman Sea has an SW monsoon climate with only 25% calms and an average wave energy of 2,806 W/m—approximately 3.25× that of the Gulf.
- C2: The base-case mooring design fatigue lifetime is 30 years for the Gulf of Thailand and 19 years for the Andaman Sea; the Gulf exceeds the conventional 25-yr target, while the Andaman Sea falls below it.
- C3: Damage accumulation is near-uniform between the two monsoon seasons at the Gulf of Thailand (NE 40%, SW 43% of annual damage) but is strongly SW-dominated at the Andaman Sea (67% of annual damage over the 5-month SW monsoon). The Gulf result reflects the cubic dependence of fatigue damage on stress range, which moderates the wave-power asymmetry that favours the NE monsoon at that site; the Andaman result confirms the dominance of the SW monsoon swell regime expected from the wave-energy distribution.
- C4: Biofouling reduces the estimated mooring design lifetime by 23–29%—a sensitivity larger than typically reported for temperate-water studies, where 10–15% effects are more common. Combined with a taut mooring configuration, the worst case drives the Andaman Sea design lifetime to 8.9 yr, below the 10-yr DNV inspection-frequency threshold. Mooring design guidance for Southeast Asian deployment should therefore require shorter biofouling-inspection intervals than cur-

rent temperate-climate standards.

- C5: Site-specific monsoon-weighted wave climate data, rather than uniformly weighted generic sea-state distributions, are essential for credible WEC mooring fatigue assessment in Southeast Asian waters.

The principal direction for future work is a fully coupled WEC-Sim assessment, driven by Thailand-specific JONSWAP spectra and including wind–current–wave coupling and a tropical corrosion–fatigue model. The framework presented here is intended as a screening tool to inform the prioritisation and design of any near-term Thai WEC pilot deployment.

Author Contributions

Conceptualization, K.R. and N.S.; methodology, K.R. and N.S.; validation, Y.T.; formal analysis, K.R.; investigation, K.R. and Y.T.; data curation, K.R.; writing—original draft preparation, K.R.; writing—review and editing, Y.T. and N.S.; visualization, K.R.; supervision, N.S.; project administration, N.S. All authors have read and agreed to the published version of the manuscript.

Funding

This research received no external funding.

Institutional Review Board Statement

Not applicable. This study did not involve humans or animals; all analyses were conducted using publicly available reanalysis datasets (ERA5, HYCOM) and secondary data from government sources (DMCR, EGAT, PEA, MEA).

Informed Consent Statement

Not applicable.

Data Availability Statement

The ERA5 reanalysis data used in this study are publicly available from the Copernicus Climate Change Service (C3S) Climate Data Store at https://cds.climate.copernicus.eu/. HYCOM ocean current data are freely accessible at https://www.hycom.org. Tide gauge data were obtained from the Marine Department, Ministry of Transport, Thailand (available upon request). Coastal erosion data are available from the Department of Marine and Coastal Resources (DMCR), Thailand, at https://www.dmcr.go.th. All processed datasets and AHP-TOPSIS calculation workbooks supporting the findings of this study are available from the corresponding author upon reasonable request.

Acknowledgments

The authors gratefully acknowledge the institutional support of Rambhai Barni Rajabhat University (RBRU), Department of Energy Technology; Kasetsart University Sriracha Campus, Department of Maritime Engineering; and Silpakorn University, Sanam Chandra Palace Campus, Department of Mechanical Engineering, which provided the research infrastructure and collaborative framework for this study. The authors also thank the editorial team and anonymous reviewers for their constructive comments, which substantially improved the quality of this manuscript, please contact Kornpaphop Ruttanawijit at kornpaphop@rbru.ac.th.

Conflicts of Interest

The authors declare that they have no known competing financial interests or personal relationships that could have appeared to influence the work reported in this paper.

AI Use Statement

The authors declare that no artificial intelligence (AI) tools were used in the preparation of this manuscript.

Abbreviations

Symbol	Definition
C	S–N curve intercept constant (MPa^k)
D	Accumulated fatigue damage (–)
D_{annual}	Annual damage rate (yr^{-1})
DFF	Design fatigue factor (–)
f	Frequency (Hz)
g	Acceleration due to gravity (9.81 m/s^2)
H_s	Significant wave height (m)
k	S–N curve slope exponent (–)
L_{est}	Estimated raw fatigue lifetime (yr)
L_{design}	Design fatigue lifetime, L_{est}/DFF (yr)
n_i	Number of stress cycles at amplitude level i (–)
N_i	Number of cycles to failure at amplitude level i (–)
$p(H_s, T_p)$	Annual joint occurrence probability of sea state (–)
S(f)	Power spectral density ($units^2$/Hz)
T_e	Wave energy period (s)
T_p	Peak wave period (s)
T_{year}	Number of seconds per year (3.156×10^7 s)
α_2	Bandwidth parameter, $\lambda_2 / \sqrt{(\lambda_0 \lambda_4)}$ (–)
γ	JONSWAP peak enhancement factor (–)
λ_n	n-th spectral moment of S(f)
ν_p	Expected peak frequency, $\sqrt{(\lambda_4/\lambda_2)}$ (Hz)
ρ	Seawater density (1,025 kg/m^3)
ρ_{mg}	Marine-growth density (1,325 kg/m^3 per DNV-OS-E301)

References

[1] Guo, B., Ringwood, J.V., 2021. A review of wave energy technology from a research and commercial perspective. IET Renewable Power Generation. 15(14), 3065–3090. DOI: https://doi.org/10.1049/rpg2.12302

[2] Astariz, S., Iglesias, G., 2015. The economics of wave energy: A review. Renewable and Sustainable Energy Reviews. 45, 397–408. DOI: https://doi.org/10.1016/j.rser.2015.01.061

[3] Penalba, M., Aizpurua, J.I., Martinez-Perurena, A., 2021. On the definition of a risk index based on long-term metocean data to assist in the design of Marine Renewable Energy systems. Ocean Engineering. 242, 110080. DOI: https://doi.org/10.1016/j.oceaneng.2021.110080

[4] Thies, P.R., Johanning, L., Harnois, V., et al., 2014. Mooring line fatigue damage evaluation for floating marine energy converters: Field measurements and prediction. Renewable Energy. 63, 133–144. DOI: https://doi.org/10.1016/j.renene.2013.08.050

[5] Xu, S., Wang, S., Soares, C.G., 2019. Review of mooring design for floating wave energy converters. Renewable and Sustainable Energy Reviews. 111, 595–621. DOI: https://doi.org/10.1016/j.rser.2019.05.027

[6] Ma, K.-T., Luo, Y., Kwan, T., et al., 2019. Fatigue analysis, in: Mooring System Engineering for Offshore Structures. Elsevier: London, UK. pp. 115–137. DOI: https://doi.org/10.1016/B978-0-12-818551-3.00006-5

[7] Yang, R., Zheng, X., Chen, J., et al., 2022. Current Status and Future Trends for Mooring Systems of Floating Offshore Wind Turbines. Sustainable Marine Structures. 4(2), 40–54. DOI: https://doi.org/10.36956/sms.v4i2.617

[8] Jiang, Z., 2025. Mooring design for floating wind turbines: A review. Renewable and Sustainable Energy Reviews. 212, 115231. DOI: https://doi.org/10.1016/j.rser.2024.115231

[9] Ruttanawijit, K., Tiaple, Y., 2026. Nearshore floating solar photovoltaic systems: A review. Maritime Technology and Research. 8(3), 284864. DOI: https://doi.org/10.33175/mtr.2026.284864

[10] Kompor, W., Ekkawatpanit, C., Kositgittiwong, D., 2018. Assessment of ocean wave energy resource potential in Thailand. Ocean & Coastal Management. 160, 64–74. DOI: https://doi.org/10.1016/j.ocecoaman.2018.04.003

[11] Foyhirun, C., Kositgittiwong, D., Ekkawatpanit, C., 2020. Wave Energy Potential and Simulation on the Andaman Sea Coast of Thailand. Sustainability. 12(9), 3657. DOI: https://doi.org/10.3390/su12093657

[12] Kanbua, W., Supharatid, S., Tang, I.-M., 2005. Ocean wave forecasting in the Gulf of Thailand during typhoon Linda 1997: Hard and soft computing approaches. Journal of Atmospheric & Ocean Science. 10(3), 145–161. DOI: https://doi.org/10.1080/17417530500359689

[13] Ekphisutsuntorn, P., Wongwises, P., Chinnarasri, C., et al., 2010. The Application of Simulating WAves Nearshore Model for Wave Height Simulation at Bangkhuntien Shoreline. American Journal of Environmental Sciences. 6(3), 299–307. DOI: https://doi.org/10.3844/ajessp.2010.299.307

[14] Kaewsai-nguan, T., Kompor, W., Thanathanphon, W., et al. Assessment of significant wave heights in Thailand using ECMWF and NCEP wind data. Journal of Engineering and Innovation. 2024. 17(3). Available from: https://ph02.tci-thaijo.org/index.php/eng_ubu/article/view/249951

[15] Martinez-Puente, E., Zarketa-Astigarraga, A., Zabala, A., et al., 2023. Fatigue Life Assessment for Wave Energy Converter Mooring Lines under Realistic Wave Climates. Proceedings of the European Wave and Tidal Energy Conference. 15. DOI: https://doi.org/10.36688/ewtec-2023-490

[16] Dirlik, T., 1985. Application of Computers in Fatigue Analysis [PhD Thesis]. University of Warwick: Coventry, UK. Available from: https://wrap.warwick.ac.uk/id/eprint/2949/1/WRAP_THESIS_Dirlik_1985.pdf

[17] Benasciutti, D., 2012. Fatigue Analysis of Random

Loadings: A Frequency-Domain Approach. LAP LAMBERT Academic Publishing: Saarbrücken, Germany. Available from: http://hdl.handle.net/11390/866212

[18] Zhang, D., Zhao, B., Jiang, H., 2024. Wave energy converter with floating-point absorber and catenary mooring: dynamic coupling analysis. Frontiers in Marine Science. 11, 1338330. DOI: https://doi.org/10.3389/fmars.2024.1338330

[19] Lou, J., Yim, S.C., Von Jouanne, A., 2024. Dynamic Mooring Field Experiment and Design of a Wave Energy Converter Platform Test System. Journal of Offshore Mechanics and Arctic Engineering. 146(1), 012001. DOI: https://doi.org/10.1115/1.4062254

[20] Xu, S., Wang, S., Guedes Soares, C., 2024. Prediction of mooring tensions of a wave energy converter considering the effects of nonlinear axial stiffness by a deep learning neural network. Ocean Engineering. 305, 117810. DOI: https://doi.org/10.1016/j.oceaneng.2024.117810

[21] Abdellatef, M., Clark, J., Kojimoto, N., et al., 2025. Wear of Wave Energy Converters Mooring Lines Belts. Journal of Offshore Mechanics and Arctic Engineering. 147(2), 022003. DOI: https://doi.org/10.1115/1.4066491

[22] Matsuishi, M., Endo, T., 1968. Fatigue of Metals Subjected to Varying Stress. Japan Society of Mechanical Engineers: Tokyo, Japan.

[23] Lee, Y.-L., Tjhung, T., 2012. Rainflow Cycle Counting Techniques, in: Metal Fatigue Analysis Handbook. Elsevier: London, UK. pp. 89–114. DOI: https://doi.org/10.1016/B978-0-12-385204-5.00003-3

[24] Park, J.-B., Choung, J., Kim, K.-S., 2014. A new fatigue prediction model for marine structures subject to wide band stress process. Ocean Engineering. 76, 144–151. DOI: https://doi.org/10.1016/j.oceaneng.2013.11.002

[25] Hersbach, H., Bell, B., Berrisford, P., et al., 2020. The ERA5 global reanalysis. Quarterly Journal of the Royal Meteorological Society. 146(730), 1999–2049. DOI: https://doi.org/10.1002/qj.3803

[26] Ruttanawijit, K., Desua, T., Tiaple, Y., 2026. Multi-Criteria Site Suitability Assessment for Nearshore Floating Solar Photovoltaic Systems in the Gulf of Thailand: Integrating Hydrodynamic, Economic, and Environmental Factors. Sustainable Marine Structures. 82–112. DOI: https://doi.org/10.36956/sms.v8i2.3210

[27] Miner, M.A., 1945. Cumulative Damage in Fatigue. Journal of Applied Mechanics. 12(3), A159–A164. DOI: https://doi.org/10.1115/1.4009458

[28] WEC-Sim Development Team, 2023. WEC-Sim (Wave Energy Converter SIMulator). Sandia National Laboratories: Albuquerque, NM, USA. Available from: https://wec-sim.github.io/WEC-Sim/main/index.html

[29] Neary, V.S., Previsic, M., Jepsen, R.A., et al., 2014. Methodology for Design and Economic Analysis of Marine Energy Conversion (MEC) Technologies. Sandia National Laboratories: Albuquerque, NM, USA. Available from: https://www.osti.gov/servlets/purl/1143279

[30] Det Norske Veritas (DNV), 2018. Offshore Standard DNV-OS-E301 – Position Mooring. DNV: Høvik, Norway.

[31] Hasselmann, K., Barnett, T.P., Bouws, E., et al., 1973. Measurements of Wind-Wave Growth and Swell Decay during the Joint North Sea Wave Project (JONSWAP). Deutsches Hydrographisches Institut (DHI): Hamburg, Germany.

[32] Det Norske Veritas (DNV), 2019. Recommended Practice DNV-RP-C205 – Environmental Conditions and Environmental Loads. DNV: Høvik, Norway.

[33] Spraul, C., Pham, H.-D., Arnal, V., et al., 2017. Effect of marine growth on floating wind turbines mooring lines responses. In Proceedings of the 23ème Congrès Français de Mécanique (CFM 2017), Lille, France, August 2017. Available from: https://hal.science/hal-04421312v1/document

[34] Iswadi, A., Porter, J.S., Bell, M.C., et al., 2022. Establishing an Agenda for Biofouling Research for the Development of the Marine Renewable Energy Industry in Indonesia. Journal of Marine Science and Engineering. 10(3), 384. DOI: https://doi.org/10.3390/jmse10030384

[35] Phuttapreecha, R., Kajonwattanakul, S., Songkai, P., et al., 2018. Survey of Fouling Organisms at Songkhla Port in Thailand. ASEAN Journal on Science and Technology for Development. 35(1–2), 147–152. DOI: https://doi.org/10.29037/ajstd.485

[36] Decurey, B., Schoefs, F., Barillé, A.-L., et al., 2020. Model of Bio-Colonisation on Mooring Lines: Updating Strategy Based on a Static Qualifying Sea State for Floating Wind Turbines. Journal of Marine Science and Engineering. 8(2), 108. DOI: https://doi.org/10.3390/jmse8020108

[37] Saputri, W.D., Pratikno, H., Sakinah, W., et al., 2025. Marine biofouling in Indonesian tropical waters: a comprehensive review of taxonomic diversity and successional dynamics. Biofouling. 41(9), 881–900. DOI: https://doi.org/10.1080/08927014.2025.2548892

[38] Portas, A., Briand, J.-F., Damblans, G., et al., 2026. A review of biofouling characteristics and issues for offshore renewable energy industry. Biofouling. 42(4), 339–360. DOI: https://doi.org/10.1080/08

927014.2026.2630946

[39] Reabroy, R., Zheng, X., Zhang, L., et al., 2019. Hydrodynamic response and power efficiency analysis of heaving wave energy converter integrated with breakwater. Energy Conversion and Management. 195, 1174–1186. DOI: https://doi.org/10.1016/j.enconman.2019.05.088

[40] Tiaple, Y., 2019. Hydrodynamic Simulation of Wave Energy Converter Using Particle-Based Computational Fluid Dynamics. Journal of Marine Science and Application. 18(1), 48–53. DOI: https://doi.org/10.1007/s11804-019-00070-0